

# A model of pan-immunity maintenance by horizontal gene transfer in the ecological dynamics of bacteria and phages

Wenping Cui,<sup>1,\*</sup> Jemma M. Fendley,<sup>2</sup> Sriram Srikant,<sup>3</sup> and Boris Shraiman<sup>1,2,†</sup>

<sup>1</sup>*Kavli Institute for Theoretical Physics, Santa Barbara, California 93106, USA*

<sup>2</sup>*Department of Physics, University of California Santa Barbara, Santa Barbara, California 93106, USA*

<sup>3</sup>*Department of Biology, Massachusetts Institute of Technology, Cambridge, Massachusetts 02139, USA*

(Dated: March 1, 2024)

Phages and their bacterial hosts are locked in an evolutionary competition which in small and closed systems typically results in the extinction of one or the other. To resist phages bacteria have evolved numerous defense systems, which nevertheless are still overcome by specific phage counter-defense mechanisms. These defense/counter-defense systems are a major element of microbial genetic diversity and have been demonstrated to propagate between strains by horizontal gene transfer (HGT). It has been proposed that the totality of defense systems found in microbial communities collectively form a distributed "pan-immune" system with individual elements moving between strains via ubiquitous HGT. Here, we formulate a Lotka-Volterra type model of a host/phage system interacting via a combinatorial variety of defense/counter-defense systems and show that HGT enables stable maintenance of diverse defense/counter-defense genes in the microbial pan-genome even when individual microbial strains inevitably undergo extinction. This stability requires the HGT rate to be sufficiently high to ensure that some descendant of a "dying" strain survives thanks to the immunity acquired through HGT from the community at large, thus establishing a new strain. This mechanism of persistence for the pan-immune gene pool is fundamentally similar to the "island migration" model of ecological diversity, with genes moving between genomes instead of species migrating between islands.

**Introduction** Bacterial viruses (phages) are the most abundant and diverse organisms on the planet. They exert substantial selection pressure on microbial communities by predation. For instance, it is estimated that marine viruses kill approximately 20% of all ocean microbes each day [1]. Facing phage predation, bacteria have developed different defense systems and strategies to interrupt the phage replication process, including restriction-modification (RM), abortive infection, and CRISPR–Cas systems [2, 3]. On the other side of this evolutionary conflict, phages have evolved counter-defense genes like the RM-inhibiting *ocr* [4, 5], protein inhibitors like *dmd* or *tifA* against abortive infection toxin-antitoxin systems [6, 7], and many different anti-CRISPR genes [8, 9].

Phages and bacteria have been a useful model to study evolution in the lab since the beginning of molecular biology. Co-culturing experiments in the lab often result in either phages or bacteria fixing in the culture driving the other to extinction [10, 11]. Further, mathematical models of such systems often show the advantageous host or phage would always dominate, and the ecosystem loses diversity unavoidably in the long run [12, 13], unless given unrealistically high mutation rates [14, 15]. However, we know that the evolutionary conflict has persisted in nature for billions of years, leading to the phylogenetic diversity we see today. Understanding the persistent coexistence of diverse hosts and phages must involve stochastic ecological dynamics coupled with evolution, in addition to the genetic systems that the two sides use

against the other [16].

Recent studies have found defense systems to be co-localized on bacterial genomes in so-called defense islands [3, 17]. Further characterization of the genomic neighborhood of defense genes in various genomes have identified their location in mobile genetic elements [18, 19]. Given the diversity and abundance of defense systems, a given genome only contains a subset of defense genes [18–20]. In several natural ecosystems, the arsenal is distributed across strains, leading to the proposition of the *pan-immunity* hypothesis, which suggests that bacteria can exchange mobile genetic elements with defense genes rapidly (henceforth referred to as HGT) to escape from selective sweep [21–24]. Phages are also limited in the number of counter-defense genes they contain due to the constraint on their packaged genome size, and therefore are limited in the number of host strains they can successfully infect [7]. Thus, phages must evolve by gaining different combinations of counter-defense genes to continue to persist in a bacterial community that is shuffling a per-genome immune profile [22, 23].

The pan-immunity hypothesis, while not yet empirically established, extends the concept of diversity into multi-level space [25]. Many of the existing models primarily focus on diversity at a single level, typically the number of surviving species [26–29]. However, the pan-immunity hypothesis emphasizes the importance of considering the diversity of genes and genotypes (strains) – combinatorial sets of different genes – separately. Since the gene space is considerably smaller than that of genotypes, it becomes more achievable for diverse genes to persist over time, regardless of the rapid extinction and turnover of genotypes.

\* wenpingcui@kitp.ucsb.edu

† shraiman@ucsb.edu

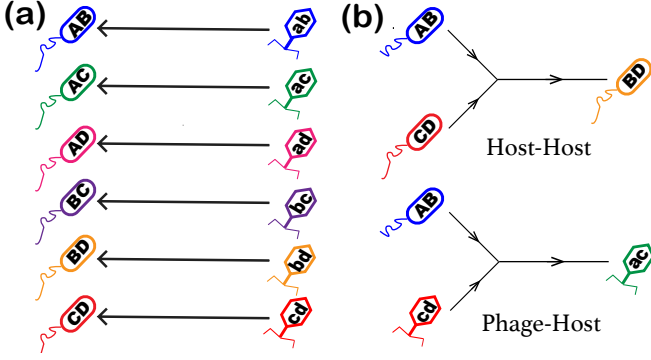


FIG. 1. **Model host and phage genotypes and HGT processes.** (a) Interaction between bacterial hosts and phages for the case of  $L = 4$  different TA systems. The capital letter denotes a specific toxin in the host; the lowercase letter denotes a corresponding antitoxin gene in the phage. Host AB will carry the toxins A and B, in addition to the antitoxins a and b. (b) Scheme for the new clone formed by host-host and phage-host HGT processes.

In this letter, we develop a stochastic Lotka-Volterra (LV) model that incorporates HGT between genotypes and explores the feasibility of pan-immunity. Our minimal model can exhibit typical LV behaviors: demographic-noise-driven extinction [30] and persistent oscillations, by changing the HGT rate. Surprisingly, between these two phases, we identify another regime where the pan-immunity hypothesis operates, and genes can persist along with the "boom-bust" dynamics of individual strains, or particular genotypes. Inspired by recent theoretical progress in islands-migration models [31], we derive novel criteria for the gene and genotype persistence regimes. Our results suggest that a relatively small HGT rate, inversely proportional to the total population size, is sufficient to maintain the coexistence of diverse genes, independent of the combinatorial diversity of genotypes, explaining how the numerous defense and counter-defense systems can persist despite strong selections in nature [32, 33].

**Model:** We shall focus on host-phage interactions assuming for simplicity that susceptibility to specific phage infection is the only heritable phenotype that affects relative fitness of host species and similarly the capacity to infect specific hosts is the only relevant distinction between phages. Thus, the relevant space of genotypes of hosts and phages is defined respectively by the defense and counter-defense genes.

To illustrate the effect of HGT, it will suffice to frame our model in the context of the toxin/antitoxin (TA) paradigm of phage defense [34]. In bacterial TA systems, toxin activity that is normally inhibited by the resident antitoxin, is triggered by phage infection leading to inhibition of phage replication. To counter this defense, phages are known to themselves acquire specific antitoxins that inhibit the TA system, allowing productive infection to proceed [6, 7]. Phages have even been shown

to acquire the antitoxin from the host TA locus by HGT [35]. The key elements of this behavior can be abstracted in terms of a toxin gene,  $A$ , and its specific antitoxin,  $a$ . A host carrying  $A$  must also carry  $a$  and, we shall assume, can only be infected by a phage carrying the antitoxin  $a$ . We shall posit the existence of a large number of distinct specific toxin/antitoxin pairs denoting them by  $L$  different uppercase/lowercase letters with  $L \gg 1$ . We emphasize that on this level of abstraction the toxin/antitoxin paradigm captures the general aspects of a broad variety of actual defense/counter-defense systems, without delving into the biochemical and genetic complexity of their mechanisms. This will suffice for our goal of providing a mathematical underpinning for the "pan-immunity" hypothesis.

Each host and phage can carry multiple defense and counter-defense genes respectively, introducing combinatorial complexity into ecological interactions. We start with each host (phage) strain carrying just two distinct TA genes. Correspondingly, there are  $K = L(L - 1)/2$  possible genotype combinations in total. Fig. 1a shows an example of  $L = 4$ , where there are  $K = 6$  possible host-phage pairs.

Let  $B_{ij}$  and  $V_{ij}$  denote the population sizes of bacteria and phage strains, respectively, with index  $ij$  specifying the genotype via the labels  $i, j$  of its TA genes. (By construction,  $B_{ij}$  and  $V_{ij}$  are symmetric with  $i \neq j$ .) The *ecological dynamics* of host and phage populations may be described by the stochastic LV equations:

$$\begin{aligned} \frac{dB_{ij}}{dt} &= sB_{ij}\left(1 - \frac{V_{ij}}{bn_G^*}\right) + \sqrt{B_{ij}}\eta_{ij}^B, \\ \frac{dV_{ij}}{dt} &= \beta sV_{ij}\left(\frac{B_{ij}}{n_G^*} - 1\right) + \sqrt{V_{ij}}\eta_{ij}^V. \end{aligned} \quad (1)$$

Here  $s$  and  $\beta s$  are the host birth rate and the phage death rate. For simplicity we neglect potential dependence of these on TA genotype  $ij$  effectively assuming all TA systems have the same intrinsic fitness cost, so that each phage/host pair follows similar dynamics.  $n_G^*$  and  $bn_G^*$  are the host and phage characteristic population sizes which parameterize the infection rate and phage burst size; specifically  $s/(bn_G^*)$  is the infection rate, and  $\beta b$  is the phage's burst size. The last term is demographic noise, and  $\eta^X$  ( $X = B, V$ ) represents the unit white noise.

As a minimal model incorporating HGT processes, we assume the host can replace one of its genes from other hosts by conjugation. Fig. 1b top shows the host recipient  $CD$  randomly acquires TA gene  $B$  from some donor  $AB$  and transforms its genotype to  $BD$ . Similarly, antitoxin genes can be passed on from one phage to another, either via (relatively rare) instances of co-infection of the same host or indirectly via a host genome as an intermediary [7]. Fig. 1b bottom shows the phage recipient can acquire an antitoxin gene from the host. Hosts and phages have HGT rates  $r$  and  $\alpha r$  (in a unit of per individual per generation), and the rates of formation of  $B_{ij}$  and  $V_{ij}$  are approximately given by  $\frac{r}{2} \sum_{k,l} B_{ik} B_{lj} / N$  for

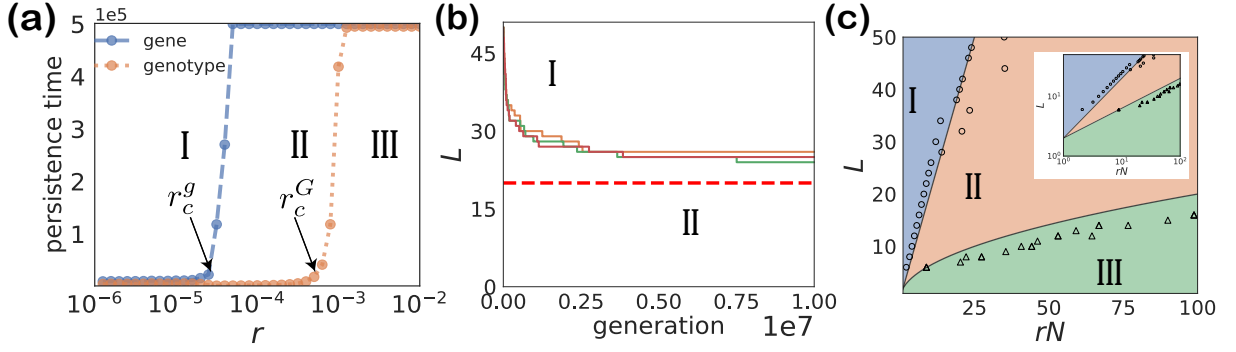


FIG. 2. **Different regimes of HGT-driven bacteria/phage dynamics.** (a) Persistence time for genes and genotypes under different HGT rate  $r$  (and fixed  $N = 10^6$  and  $L = 40$ ). Persistence time is defined by the simulation time (averaged over 5 trials) until the first gene or genotype is lost (with the upper limit at generation  $T = 5 \times 10^5$  imposed by the maximum simulation length). (b) Genetic diversity decreases when its initial value exceeds  $L_{max}$  (for  $N = 10^6$  and  $r = 2 \times 10^{-5}$ ). The solid lines are from 3 trials of simulations. The red dashed line is  $L_{max} = rN$  given by our theory. (c) Parameter regimes corresponding to three qualitatively different behaviors: I: unstable coexistence; II: persistence of genes with continuous turnover of genotypes; III: stable coexistence; the circle and triangle markers represent simulations at the transition boundary between I/II and II/III, respectively. The inset shows the same data but on a log-log scale. The black solid lines separating different regimes are our theoretical predictions  $L_{max} = rN$  (upper) and  $K_{max} = rN$  (lower), respectively. Our default simulation parameters are  $N = 10^6$ ,  $L = 40$ ,  $K = 780$ , and  $s = 5 \times 10^{-3}$  unless specified otherwise.

host-host HGT and  $\frac{\alpha r}{4} \sum_{k,l} (V_{ik} B_{lj}/N + V_{lj} B_{ik}/N)$  for phage-host HGT. Here  $N$  is the total population size of the hosts. The summary of notations and the full description of our simulation can be found at Supplementary Information (SI) Sec. I & II.

The two-species LV dynamics can always be rescaled to the anti-symmetric form [31, 36]. To further simplify our analysis, we choose the perfectly anti-symmetric form by setting  $\alpha = \beta = b = 1$ . Without the loss of generality, we enforce a constraint on the total population size with  $N = Kn_G^*$  for the hosts and phages. In SI Sec. VIII, we investigate the generalized parameters setting, and our analysis suggests that it has no significant impact on our primary findings (also see Fig. S8, Fig. S11).

**Different regimes in the dynamics of genes and genotypes:** We would like to understand how HGT processes affect the distribution of (host and phage) genotypes and the frequencies of specific TA genes in the pan-genome. Fig. 2a shows how long the system keeps its full gene and genotype diversity when all genotypes start from the mean population size  $N/K$ . Numerical simulations reveal three distinct regimes as a function of the HGT rate  $r$ , and thus two critical HGT rates  $r_c^g$  and  $r_c^G$  are defined with  $r_c^g < r_c^G$ .

*Regime I* is the *unstable-coexistence* regime which occurs for low HGT rate  $r < r_c^g$ . In this regime any given strain (i.e. a particular  $ij$  genotype) persists for a short time before going extinct and is unlikely to reappear via HGT. Loss of genotypes leads to a loss of genes (see Fig. 2a), reducing genetic diversity. The host/phage system keeps losing genetic diversity until the "birth rate" of genotypes via HGT is sufficient to compensate the loss of genotypes under selection. The genetic diversity will then be sustained, but with a smaller number of genes (i.e. TA

systems),  $L_{max}$  (see Fig. 2b), and a larger average population size of different genotypes. Thus the unstable-coexistence regime appears transiently while  $L > L_{max}$ , as shown in Fig. 2b, with the dependence of  $L_{max}$  on  $rN$  defining the boundary of the unstable coexistence regime in the phase diagram Fig. 2c.

*Regime II* is the regime of *genotype turnover* and gene persistence, which occurs in the intermediate range of HGT rate  $r_c^g < r < r_c^G$ . In this regime host-phage pairs undergo *boom-bust* behavior: a newly established host genotype, formed by HGT, grows rapidly until infected by a phage which subsequently leads to a "crash", and then goes extinct.

Critically, however, in this regime the HGT rate is high enough for one or more descendants of the clonal population to acquire immunity against the phage, via a horizontally-transferred TA gene. A successful transfer event establishes a new immune genotype, which will subsequently undergo a boom-bust cycle of its own. Fig. 3a shows that the genotypes have a short lifetime, but HGT enables TA genes to persist in the pan-genome of the community, effectively "surfing" from one boom-bust wave to another. This regime provides a model for the pan-immunity hypothesis. Only a fraction of all possible genotypes exist at any instant of time; however, the system can still maintain genetic diversity by distributing genes across the community.

*Regime III* is the regime of *genotype persistence* realized at a sufficiently high HGT rate  $r > r_c^G$ . Fig. 3d shows the host-phage pair undergoing *stochastic oscillations* around a well defined mean population size without going extinct. In this regime frequent HGT spreads host and phage genotypes over all available genotypes, making immune escape impossible, while also eliminating large

boom-bust events. This is the endemic infection regime, which is also the regime of stable host-phage coexistence.

Our simulations further demonstrate that the critical HGT rates  $r_c^g$  and  $r_c^G$  depend only on the total population size  $N$  and the genetic diversity  $L$ . Consequently, we can alternatively express the critical curves for a given  $N$  and  $r$  in terms of  $L_{max}$ , representing the maximum genetic diversity and analogous to the carrying capacity in ecology. If the initial value of  $L$  is larger than  $L_{max}$ , the system starts at Regime I, which is unstable, and subsequently slides toward the edge of Regime II, as illustrated in Fig. 2b. Likewise, we also have the maximum genotypic diversity  $K_{max}$ , conditioned upon the coexistence of all possible genotypes, lying at the boundary between Regime II and Regime III. Fig. 2c provides the full phase diagram (we transform  $K_{max}$  back to its corresponding  $L$  for comparison in the same diagram), and we will give our theoretical analysis about the critical curves in the following sections.

**Phage/host "ensemble":** What is the critical value of  $r$  for the transition between regimes, given model parameters? To identify suitable observable quantities to describe the irregular and coupled population dynamics of many phage-host pairs in Fig. 3ad, we shall follow Goel *et al.*, as our system in eqs. (1) falls into a broad class of anti-symmetric LV models investigated before [31, 36]. It is useful to define the Lyapunov function [36] for a single host-phage pair as

$$E(B, V) = (B - n_G^* \log \frac{B}{n_G^*}) + (V - n_G^* \log \frac{V}{n_G^*}), \quad (2)$$

which characterizes the distance between the current state and the steady state. In the deterministic limit  $N \rightarrow \infty$ ,  $E$  is determined by the initial condition and does not change with time, corresponding to a host/pathogen population undergoing a neutrally stable periodic oscillation.

In the spirit of statistical mechanics, one may interpret  $E$  as the energy of a "particle", and describe the state of the stochastic LV system with a large number of interacting strains by a canonical ensemble [36, 37]. In our case HGT processes play a role similar to particle collisions for energy exchange. Then the probability density function (PDF) of microstates follows Boltzmann statistics which give the *Gamma* distribution:

$$n_G \sim \Gamma(\frac{N}{K}, \Theta) = \frac{n_G^{\frac{N}{K\Theta}-1} e^{-n_G/\Theta}}{\Theta^{\frac{N}{K\Theta}} \Gamma(\frac{N}{K\Theta})}. \quad (3)$$

For simplicity, we use  $n_G$  to represent either host or phage abundances since their distributions have the same general form. The mean is given by  $N/K$  and  $\Theta$  is an unknown effective temperature for genotypes, characterizing the fluctuations of genotype abundances.

The gene abundance  $n_g$  is the sum of population sizes of all extant genotypes containing specific gene  $g$ . We assume the Gamma distribution ansatz can also be applied to the gene abundance:  $n_g \sim \Gamma(2N/L, \theta)$ , where  $2N/L$

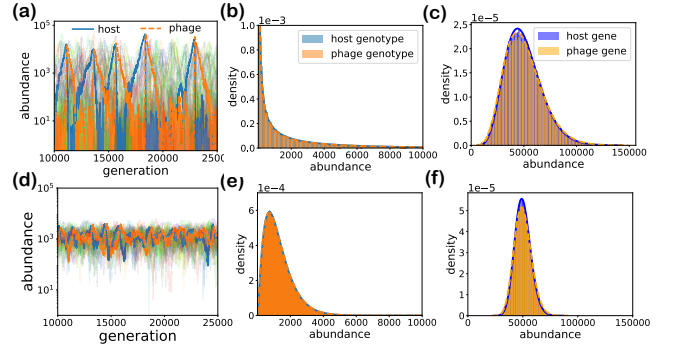


FIG. 3. **Phage/host population dynamics and the distributions of genes and genotypes in Regimes II and III.** (a, d) Time course of multiple phage (orange dashed lines) and host (blue solid lines) populations. One phage/host-pair is emphasized to illustrate distinct dynamics in Regime II ( $r = 5 \times 10^{-5}$ ) and Regime III ( $r = 10^{-3}$ ) in (a) and (d) respectively. Corresponding genotype (b, e) and gene (c, f) abundance distributions. Dashed lines are the fitted Gamma distributions.

is the mean gene abundance (the factor 2 arising from two-gene genotypes), and  $\theta$  is another unknown effective temperature for genes.

Fig. 3 shows that Gamma distributions provide an excellent fit of the genotype and gene abundance distributions across Regime II and III, even though their population dynamics behave quite differently.

**"Effective temperatures" for genes and genotypes:** We next address the relationship between the effective temperatures,  $\theta$  and  $\Theta$ , that describe phage/host statistics within the canonical ensemble framework, with the parameters controlling phage/host dynamics.

The HGT process can be approximated in the mean-field sense by adding a constant  $rN/K$  source term into both of eqs. (1). This is because the sampling probability of a specific genotype from HGT is proportional to the product of marginal probabilities of genes it carries [38]; at the genotype scale, the fluctuations of gene abundances can be averaged out with the law of large numbers (also see simulations in SI Fig. S9), suggesting the new clones can be uniformly sampled over the whole genotype space. Within this approximation, the effect of HGT on ecological dynamics is similar to the effect of "island migration", extensively studied in the context of LV models of ecological dynamics [31].

Using Itô's lemma [39], we can write down the Lyapunov function dynamics for eqs. (1) with the additional terms for the constant rate of genotype generation from HGT:

$$dE = \left( \frac{n_G^*}{2B} + \frac{n_G^*}{2V} - r \frac{N(n_G^*-B)}{KB} - r \frac{N(n_G^*-V)}{KV} \right) dt + \sqrt{\frac{(B-n_G^*)^2}{B} + \frac{(V-n_G^*)^2}{V}} d\eta. \quad (4)$$

From the above equation, we see that demographic noise contributes a positive drift and drives  $E$  to grow expo-



nentially (see SI Sec. IV). The injection of new clones due to HGT processes contributes a balancing force to cancel the effect of demographic noise and stabilizes the system.

Without HGT, the demographic noise drives the system away from the steady state. The oscillation amplitude grows until either the host or the phage dies out and the coexistence becomes unstable after a typical persistence time proportional to the average clone size  $N/K$  (see SI Sec. IV and Fig. S2). Once any phage goes extinct first, its corresponding host becomes advantageous and drives the catastrophic extinction of other hosts because of competitive exclusion.

In Regime III where  $r$  is sufficiently large, the system is stable and the average of  $E$  does not change in thermal equilibrium. We then obtain  $\Theta = \frac{1}{2r}$  by solving the self-consistency relation that the drift part averaged over the canonical ensemble is zero. With similar calculations for the mean-field gene dynamics derived from quasi-linkage equilibrium [38], we obtain  $\theta = \frac{2}{r}$ , larger than  $\Theta$ . This is because the sampling space of the host-host HGT tends to concentrate on the genotypes containing abundant genes. The biased sampling can be written as a quadratic term in the mean field approximation, resulting in stronger fluctuations at the gene level than the genotype level (see SI Sec. V for more details).

However, our previous analysis does not work for Regime II since either the phage or the host can go extinct, and the Lyapunov function  $E$  is no longer well defined. Fig. 3a shows that most strains have small population sizes, represented by a large pile-up near zero, while a few booming strains dominate in the system, represented by an exponential tail in the right. We can just focus on the booming strains, and the exponential tail in the Gamma distribution suggests they have a typical population size (peak size)  $\sim \Theta$  [31].

We next estimate the typical peak size of the booming strains by connecting the "kill-the-winner" mechanism [14, 40, 41] with the establishment probability in population genetics [42, 43] as follows: the booming host has an approximately constant fitness  $s$  as long as its corresponding phage population is small. Hence, the host (after establishing itself with the population size  $\frac{1}{2s}$ ) follows deterministic exponential growth  $e^{st}$  until the phage with antitoxin genes that enable infection of this host emerges due to HGT and is itself established [42] (see Fig. S3). Since the boom-bust cycles show that, most of the time, the phage barely interferes with the susceptible host, we can use branching processes to evaluate the phage's establishment probability conditioned on the susceptible host's instantaneous abundance [44]. Then considering the constant rebirth rate  $rN/K$  for one specific phage strain along with its probability of establishment, we can estimate the waiting time for the first phage to get established [42]. Upon establishment, given the large abundance of the host at this time, the established phage proliferates rapidly, leading to the immediate decline of the susceptible host population. Consequently, the host

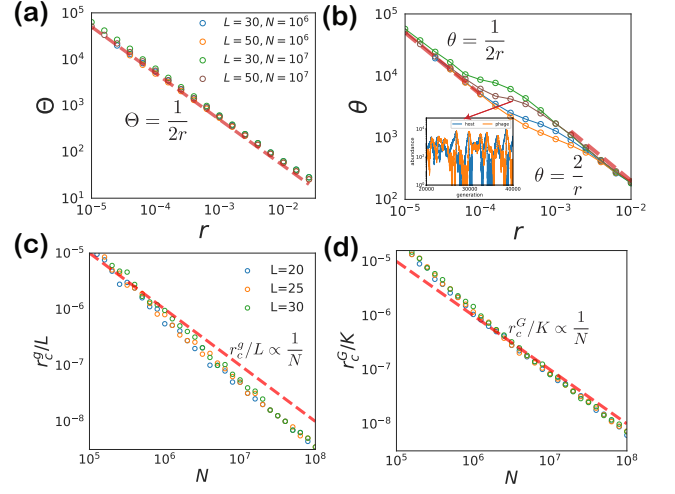


FIG. 4. "Effective temperatures" and critical HGT rates. (a, b) The scaling of  $\Theta$  and  $\theta$  in Gamma distributions of genotype and gene abundances at different HGT rates  $r$ . Red dashed lines are theoretical predictions. Inset in (b) shows an example of a phage-host pair exhibiting a mixture of boom-bust and stochastic-oscillation dynamics at the crossover between Regimes II and III. (c, d) Critical (minimal) HGT rates for gene and genotype coexistence. The red dashed lines are our predictions. All data points are simulations with gene (c) or genotype (d) persistence time over  $2 \times 10^5$  generations.

population size at the time of the phage's establishment can be used to determine its typical peak size. Our analysis (see SI Sec. VI and Fig. S4 for details) shows that the peak size follows an exponential distribution with exponential rate  $-2r$ , yielding  $\Theta \approx \frac{1}{2r}$ . In this regime, as  $r$  is small, different booming strains are weakly correlated and the gene abundance distribution is approximated by the sum of  $L - 1$  independent Gamma distribution for genotypes, which is still a Gamma distribution with the same exponential tail, yielding  $\theta = \Theta = \frac{1}{2r}$ .

In summary, our analysis of the dynamical behavior suggests the following scaling:

$$\begin{cases} \Theta = \theta = \frac{1}{2r} & \text{for boom-bust cycles} \\ \Theta = \frac{1}{2r}, \quad \theta = \frac{2}{r} & \text{for stochastic oscillations} \end{cases} \quad (5)$$

which match well with numerics in Fig. 4ab. Fig. 4b also shows the system can exhibit mixed dynamics when  $\theta$  changes smoothly from  $\frac{1}{2r}$  to  $\frac{2}{r}$  in the transition from Regime II to III, consistent with our theory.

**Critical values of  $r$  and generalizations:** The shape of the PDF for genes and for genotypes provides a natural criteria designating different regimes: the power exponent (in eq. (3)) must be positive in order to avoid the PDF diverging at  $n_G = 0$  or  $n_g = 0$ , which requires that

$$\frac{N}{K\Theta} - 1 > 0 \text{ and } \frac{2N}{L\theta} - 1 > 0. \quad (6)$$

Otherwise, the mode of the PDF is at zero, corresponding to an extinction of the genotype or gene. Hence the

equalities  $\frac{N}{K\Theta} = 1$  and  $\frac{2N}{L\theta} = 1$  demarcate transitions between I/II and II/III respectively. Given the scaling of  $\Theta$  and  $\theta$  in eqs. (5), the minimal  $r$  to maintain gene and genotype diversity are

$$r_c^g \propto \frac{L}{N} \text{ and } r_c^G \propto \frac{K}{N}. \quad (7)$$

While this scaling is robust the argument does not determine the pre-factor (which is order 1); gene and genotype abundance fluctuate strongly near respective transitions, invalidating the mean-field theory assumptions that we have made in treating HGT (see SI Fig. S6). Overall, as shown in Fig. 4cd, eqs. (7) agree well with the results of numerical simulations. Alternatively we can define transitions in terms of  $L$  as a function of total population size  $N$  and HGT rate  $r$ . Equations (7) imply that  $L_{max}$  and  $K_{max}$  at the transitions are proportional to  $rN$  – a result confirmed by numerical simulations in Fig. 2c.

The transition criteria defined above are quite general. As an example, we consider the transition to the gene maintenance regime for the case with "tripleton" genotypes, i.e. each genotype carrying three genes so that  $K \propto L^3$  in contrast to  $K \propto L^2$  for the "doubleton" case analyzed above. Fig. 4 and Fig. S10 show that the HGT rate required to maintain genetic diversity only grows linearly with the number of genes, in contrast to the faster polynomial (in  $L$ ) growth of the genotype space. We can understand this from our criteria for gene persistence, which gives  $rN$  as the estimate for the number of booming hosts (each with a typical population size of order of  $1/r$ ). This number must exceed  $L$  so that there are enough booming strains to carry all genes to escape from selective sweep, regardless of the "doubleton" or "tripleton" structure of the genotype.

As there are multiple ways for phages and hosts to acquire genes [7], we also consider the effect of phage-phage HGT as the dominant mechanism for generating "new" phages (see SI Sec. VII). The mean-field theory description of HGT as a constant source of genotypes still applies, and Fig. S6 shows that eqs. (7) remain valid. However, when  $r$  is large like in Regime III, the difference between phage-host and phage-phage HGT becomes significant at the gene level, but they are indistinguishable at the genotype level as the gene and genotype dynamics are still decoupled (see the summary of "effective temperature" in Table I). With phage-phage HGT, a scenario arises where if the phage community loses a single anti-toxin gene, hosts carrying the corresponding toxin gene gain a perpetual advantage under selection. This can result in catastrophic extinctions of other hosts. This situation (which is unlikely when  $rN > L$ ), is of course mitigated by any low rate of host-phage HGT or new anti-toxin emergence via de novo mutation (not considered in the present analysis).

**Discussion:** In this letter, we have formulated and explored a simple model of phage-host competition driven by host defense and phage counter-defense systems, focusing on the role of HGT in maintaining gene diversity.

For simplicity sake we have framed the model in terms of combinatorial variety of defense systems built of different "flavors" of toxin and antitoxin genes, with specific pairwise interactions. It would be possible to extend our model to handle a heterogeneous set of defense/counter-defense systems, appearing in different combinations and with different level of specificity. There is, however, firm evidence of phages acquiring parts of host defense systems enabling productive infection. For example, phages often encode methylase genes homologous to bacterial RM systems to gain resistance to such systems [45]. Another example is provided by CRISPR-Cas immunity; work showed that phages can acquire CRISPR repeat-spacer sequences to inhibit the formation of functional CRISPR machinery in a host [46].

Our analysis was focused on the feasibility of maintaining diversity in the presence of frequent extinction (of individual strains and their genotypes) solely by the virtue of HGT, even without the effect of mutation. The latter is of course well known to play an essential role in host-pathogen coevolution, e.g. mutations in host and phage proteins abrogate or restore their specific interaction [47, 48]. The "Red Queen" dynamics of such competitive coevolution can be folded into a suitably generalized model and would partially stabilize host/pathogen strains by reducing the effective rate of extinction. This would effectively push the host pathogen system towards the endemic coexistence in Regime III of our phase diagram.

The importance of HGT processes in ecological dynamics and evolution of microbial communities is now broadly recognized [49]. HGT appears to be ubiquitous in nominally asexual microbes with an estimated rate comparable to the rate of mutation [50]. Frequent HGT effectively unlinks genes from genomes, enabling selection to act on genes in the community metagenome, much like it does in linkage quasi-equilibrium in sexually reproducing populations [38]. In this sense, the pool of TA genes forming the pan-immunity resource of the microbial community is maintained by selection through the boom/bust cycles of our Regime II.

Our model of pan-immunity is closely related to the multiple-islands-migration model in [31]. Genes and genotypes are analogous to strains and "islands", respectively, and HGT plays a similar role as migration to stabilize the phage-host dynamics. The spatial structure in their model is replaced with a genetic structure in ours, which allows for different applications.

Our study demonstrates that, given the huge microbial population size and frequent HGT events within individuals, the pan-immunity hypothesis allows for the persistence of diverse genes. This combination of diverse genes contributes to a high-dimensional genotype space, leading to the emergence of numerous unoccupied "micro-niches", particularly when the interactions between defense and counter-defense genotypes are sparse (a more general scenario where a single host can be infected by multiple distinct phages is shown in Fig. S12). Our re-

sults imply that a small number of thriving strains is sufficient to back up diverse genes. These strains undergo rapid turnover among vast micro-niches, and the phage-host arms race never ends.

**Acknowledgments:** The authors gratefully acknowledge stimulating discussions with Fridtjof Brauns, Tong Wang, Thierry Mora and Aditya Mahadevan. WC acknowledges support via NSF PHY:1748958, GBMF

Grant No. 2919.02, and Simons Foundation. BIS acknowledges support via NSF PHY:1707973 and NSF PHY:2210612, S.S. is a Howard Hughes Medical Institute Awardee of the Life Sciences Research Foundation. WC also acknowledges generous help from Pankaj Mehta. The numeric results reported in this manuscript are performed on the Shared Computing Cluster of Boston University and UCSB Center for Scientific Computing.

- 
- [1] C. A. Suttle, Marine viruses—major players in the global ecosystem, *Nature reviews microbiology* **5**, 801 (2007).
  - [2] R. Barrangou, C. Fremaux, H. Deveau, M. Richards, P. Boyaval, S. Moineau, D. A. Romero, and P. Horvath, Crispr provides acquired resistance against viruses in prokaryotes, *Science* **315**, 1709 (2007).
  - [3] S. Doron, S. Melamed, G. Ofir, A. Leavitt, A. Lopatina, M. Keren, G. Amitai, and R. Sorek, Systematic discovery of antiphage defense systems in the microbial pangenome, *Science* **359**, eaar4120 (2018).
  - [4] C. Atanasiu, O. Byron, H. McMiken, S. Sturrock, and D. Dryden, Characterisation of the structure of ocr, the gene 0.3 protein of bacteriophage t7, *Nucleic Acids Research* **29**, 3059 (2001).
  - [5] M. Walkinshaw, P. Taylor, S. Sturrock, C. Atanasiu, T. Berge, R. M. Henderson, J. Edwardson, and D. Dryden, Structure of ocr from bacteriophage t7, a protein that mimics b-form dna, *Molecular cell* **9**, 187 (2002).
  - [6] Y. Otsuka and T. Yonesaki, Dmd of bacteriophage t4 functions as an antitoxin against escherichia coli lsoa and rnlx toxins, *Molecular microbiology* **83**, 669 (2012).
  - [7] S. Srikant, C. K. Guegler, and M. T. Laub, The evolution of a counter-defense mechanism in a virus constrains its host range, *eLife* **11**, e79549 (2022).
  - [8] J. Bondy-Denomy, A. Pawluk, K. L. Maxwell, and A. R. Davidson, Bacteriophage genes that inactivate the crispr/cas bacterial immune system, *Nature* **493**, 429 (2013).
  - [9] A. Pawluk, A. R. Davidson, and K. L. Maxwell, Anti-crispr: discovery, mechanism and function, *Nature Reviews Microbiology* **16**, 12 (2018).
  - [10] R. E. Lenski and B. R. Levin, Constraints on the coevolution of bacteria and virulent phage: a model, some experiments, and predictions for natural communities, *The American Naturalist* **125**, 585 (1985).
  - [11] J. M. Borin, J. J. Lee, A. Lucia-Sanz, K. R. Gerbino, J. M. Weitz, and J. R. Meyer, Rapid bacteria-phage coevolution drives the emergence of multi-scale networks, *bioRxiv*, 2023 (2023).
  - [12] L. M. Childs, W. E. England, M. J. Young, J. S. Weitz, and R. J. Whitaker, Crispr-induced distributed immunity in microbial populations, *PLoS one* **9**, e101710 (2014).
  - [13] S. Pilosof, S. A. Alcalá-Corona, T. Wang, T. Kim, S. Maslov, R. Whitaker, and M. Pascual, The network structure and eco-evolutionary dynamics of crispr-induced immune diversification, *Nature Ecology & Evolution* **4**, 1650 (2020).
  - [14] C. Xue and N. Goldenfeld, Coevolution maintains diversity in the stochastic “kill the winner” model, *Physical review letters* **119**, 268101 (2017).
  - [15] S. Martis, Eco-evolutionary feedback can stabilize diverse predator-prey communities, *bioRxiv*, 2022 (2022).
  - [16] A. Chevallereau, B. J. Pons, S. van Houte, and E. R. Westra, Interactions between bacterial and phage communities in natural environments, *Nature Reviews Microbiology* **20**, 49 (2022).
  - [17] L. Gao, H. Altae-Tran, F. Böhning, K. S. Makarova, M. Segel, J. L. Schmid-Burgk, J. Koob, Y. I. Wolf, E. V. Koonin, and F. Zhang, Diverse enzymatic activities mediate antiviral immunity in prokaryotes, *Science* **369**, 1077 (2020).
  - [18] F. Rousset, J. Dowding, A. Bernheim, E. P. Rocha, and D. Bikard, Prophage-encoded hotspots of bacterial immune systems, *bioRxiv*, 2021 (2021).
  - [19] C. N. Vassallo, C. R. Doering, M. L. Littlehale, G. I. Teodoro, and M. T. Laub, A functional selection reveals previously undetected anti-phage defence systems in the e. coli pangenome, *Nature microbiology* **7**, 1568 (2022).
  - [20] D. Hochhauser, A. Millman, and R. Sorek, The defense island repertoire of the escherichia coli pan-genome, *PLoS genetics* **19**, e1010694 (2023).
  - [21] K. M. Kauffman, W. K. Chang, J. M. Brown, F. A. Hussain, J. Yang, M. F. Polz, and L. Kelly, Resolving the structure of phage–bacteria interactions in the context of natural diversity, *Nature communications* **13**, 372 (2022).
  - [22] K. N. LeGault, S. G. Hays, A. Angermeyer, A. C. McKittrick, F.-t. Johura, M. Sultana, T. Ahmed, M. Alam, and K. D. Seed, Temporal shifts in antibiotic resistance elements govern phage-pathogen conflicts, *Science* **373**, eabg2166 (2021).
  - [23] D. Piel, M. Bruto, Y. Labreuche, F. Blanquart, D. Goudenège, R. Barcia-Cruz, S. Chenivesse, S. Le Panse, A. James, J. Dubert, *et al.*, Phage–host coevolution in natural populations, *Nature Microbiology* **7**, 1075 (2022).
  - [24] A. Bernheim and R. Sorek, The pan-immune system of bacteria: antiviral defence as a community resource, *Nature Reviews Microbiology* **18**, 113 (2020).
  - [25] L. M. Childs, N. L. Held, M. J. Young, R. J. Whitaker, and J. S. Weitz, Multiscale model of crispr-induced coevolutionary dynamics: diversification at the interface of lamark and darwin, *Evolution* **66**, 2015 (2012).
  - [26] G. Bunin, Ecological communities with lotka-volterra dynamics, *Physical Review E* **95**, 042414 (2017).
  - [27] W. Cui, R. Marsland III, and P. Mehta, Effect of resource dynamics on species packing in diverse ecosystems, *Physical review letters* **125**, 048101 (2020).
  - [28] G. Biroli, G. Bunin, and C. Cammarota, Marginally stable equilibria in critical ecosystems, *New Journal of Physics* **20**, 083051 (2018).

- [29] C. A. Serván, J. A. Capitán, J. Grilli, K. E. Morrison, and S. Allesina, Coexistence of many species in random ecosystems, *Nature ecology & evolution* **2**, 1237 (2018).
- [30] A. Dobrinevski and E. Frey, Extinction in neutrally stable stochastic lotka-volterra models, *Physical Review E* **85**, 051903 (2012).
- [31] M. T. Pearce, A. Agarwala, and D. S. Fisher, Stabilization of extensive fine-scale diversity by ecologically driven spatiotemporal chaos, *Proceedings of the National Academy of Sciences* **117**, 14572 (2020).
- [32] A. A. Hossain, J. McGinn, A. J. Meeske, J. W. Modell, and L. A. Marraffini, Viral recombination systems limit crispr-cas targeting through the generation of escape mutations, *Cell Host & Microbe* **29**, 1482 (2021).
- [33] F. A. Hussain, J. Dubert, J. Elsherbini, M. Murphy, D. Vaninsberghe, P. Arevalo, K. Kauffman, B. K. Rodino-Janeiro, H. Gavin, A. Gomez, *et al.*, Rapid evolutionary turnover of mobile genetic elements drives bacterial resistance to phages, *Science* **374**, 488 (2021).
- [34] M. LeRoux and M. T. Laub, Toxin-antitoxin systems as phage defense elements, *Annual review of microbiology* **76**, 21 (2022).
- [35] T. R. Blower, T. J. Evans, R. Przybiski, P. C. Fineran, and G. P. C. Salmond, Viral evasion of a bacterial suicide system by rna-based molecular mimicry enables infectious altruism, *PLOS Genetics* **8**, 1 (2012).
- [36] N. S. Goel, S. C. Maitra, and E. W. Montroll, On the volterra and other nonlinear models of interacting populations, *Reviews of modern physics* **43**, 231 (1971).
- [37] E. H. Kerner, A statistical mechanics of interacting biological species, *The bulletin of mathematical biophysics* **19**, 121 (1957).
- [38] R. A. Neher and B. I. Shraiman, Statistical genetics and evolution of quantitative traits, *Reviews of Modern Physics* **83**, 1283 (2011).
- [39] C. W. Gardiner *et al.*, *Handbook of stochastic methods*, Vol. 3 (springer Berlin, 1985).
- [40] M. Doebeli, E. C. Jaque, and Y. Ispolatov, Boom-bust population dynamics increase diversity in evolving competitive communities, *Communications Biology* **4**, 502 (2021).
- [41] S. Maslov and K. Sneppen, Population cycles and species diversity in dynamic kill-the-winner model of microbial ecosystems, *Scientific reports* **7**, 1 (2017).
- [42] M. M. Desai and D. S. Fisher, Beneficial mutation–selection balance and the effect of linkage on positive selection, *Genetics* **176**, 1759 (2007).
- [43] R. A. Neher, B. I. Shraiman, and D. S. Fisher, Rate of adaptation in large sexual populations, *Genetics* **184**, 467 (2010).
- [44] R. A. Neher, C. A. Russell, and B. I. Shraiman, Predicting evolution from the shape of genealogical trees, *Elife* **3**, e03568 (2014).
- [45] J. Murphy, J. Mahony, S. Ainsworth, A. Nauta, and D. van Sinderen, Bacteriophage orphan dna methyltransferases: insights from their bacterial origin, function, and occurrence, *Applied and environmental microbiology* **79**, 7547 (2013).
- [46] S. Camara-Wilpert, D. Mayo-Muñoz, J. Russel, R. D. Fagerlund, J. S. Madsen, P. C. Fineran, S. J. Sørensen, and R. Pinilla-Redondo, Bacteriophages suppress crispr–cas immunity using rna-based anti-crisprs, *Nature* , 1 (2023).
- [47] L. Yan, R. A. Neher, and B. I. Shraiman, Phylodynamic theory of persistence, extinction and speciation of rapidly adapting pathogens, *Elife* **8**, e44205 (2019).
- [48] J. Marchi, M. Lässig, A. M. Walczak, and T. Mora, Antigenic waves of virus–immune coevolution, *Proceedings of the National Academy of Sciences* **118**, e2103398118 (2021).
- [49] B. J. Arnold, I.-T. Huang, and W. P. Hanage, Horizontal gene transfer and adaptive evolution in bacteria, *Nature Reviews Microbiology* **20**, 206 (2022).
- [50] M. J. Rosen, M. Davison, D. Bhaya, and D. S. Fisher, Fine-scale diversity and extensive recombination in a quasisexual bacterial population occupying a broad niche, *Science* **348**, 1019 (2015).
- [51] D. T. Gillespie, Approximate accelerated stochastic simulation of chemically reacting systems, *The Journal of chemical physics* **115**, 1716 (2001).
- [52] B. Ottino-Löffler and M. Kardar, Population extinction on a random fitness seascape, *Physical Review E* **102**, 052106 (2020).
- [53] T. Agranov and G. Bunin, Extinctions of coupled populations, and rare event dynamics under non-gaussian noise, *Physical Review E* **104**, 024106 (2021).
- [54] D. L. Snyder and M. I. Miller, *Random point processes in time and space* (Springer Science, 2012).



# Supplementary Information

## CONTENTS

References	7
I. Summary of notation	9
II. Simulation	10
III. Canonical ensemble and Gamma distribution ansatz	10
1. Surviving fraction	11
IV. Stochastic LV model without horizontal gene transfer	12
V. Regime III: stochastic oscillation with high HGT rates	13
1. Stochastic Lotka-Volterra equations with HGT	13
2. Self-consistency relations	13
a. Solution of $\Theta$ and critical point	13
b. An alternative explanation from LV dynamics	14
VI. Regime II: boom-bust cycles with low HGT rates	14
1. Establishment (fixation) probability in a changing environment	14
2. Sampling from HGT	16
3. Consistency with canonical ensemble	16
4. Booming duration and time gap between consecutive booms	17
5. Mean population size without the population size constraint	18
VII. Different mechanisms of horizontal gene transfer	18
1. Ideal mean-field case	18
2. Host-host and phage-host HGT	20
a. Decoupling of gene and genotype dynamics	20
3. Host-host and phage-phage HGT	21
a. Effective genotype temperature	22
4. Summary	22
VIII. Distinct parameters for hosts and phages	23
1. Regime III	23
2. Summary	24
IX. Transformation between the time and population distributions	25
X. Establishment probability with a constant fitness for two different processes	25
1. Birth-death process	25
2. Poisson process	25
XI. Supplementary figures	26

## I: Summary of notation

We summarize the notation that appeared in the main text and supplemental information:

$B$	Bacterial host genotype population size
$V$	Bacterial phage (virus) genotype population size
$L$	Number of genes. We always assume phages and hosts have the same number of different genes
$K$	Number of genotypes, $K = \binom{L}{2} = L(L-1)/2$ for "doubleton"; for $K = \binom{L}{3}$ for "tripleton"
$N_B, N_V$	Total population sizes for the hosts and phages. We set $N = N_B = N_V$ in the main text.

$s_B, s_V$	The host intrinsic growth rate; the phage death rate. We set $s = s_B = s_V$ in the main text.
$r_B, r_V$	HGT rates for hosts and phages. We set $r = r_B = r_V$ in the main text.
$n_G$	Genotype abundance, no distinction for hosts and phage
$n_G^*$	Average population size for one specific genotype, $n_G^* = N/K$ . If the host and phage are assumed to have different fixed points, we use $n_B^*$ and $n_V^*$ to represent them.
$n_g$	Gene abundance, no distinction for defense and counter-defense systems
$n_g^*$	Average population size for one specific gene, $n_g^* = 2N/L$ for "doubleton"
$\Theta$	Effective temperature for Boltzmann (Gamma) distribution of genotype abundances
$\theta$	Effective temperature for Boltzmann (Gamma) distribution of gene abundances
$E$	Lyapunov function, defined in eq. (III1)
$\alpha$	The ratio between the phage and host HGT rates, $\alpha = r_V/r_B$
$\beta$	The ratio between the phage's death rate and the host's intrinsic growth rate, $\beta = s_V/s_B$
$b$	The ratio between the total phage and host population sizes, $b = N_V/N_B$

We would like to note that we assume hosts and phage have anti-symmetric parameters so that they share the same statistical properties. If the host and phage have different parameters, we use notations  $X_B$  and  $X_V$  ( $X$  could be  $s, N, r$ ).

## II: Simulation

We must consider stochastic effects when the population size is finite. We use the  $\tau$ -leaping method [51] to simulate eqs. (1) in the main text:

$$B_{ij}^{t+1} = \text{Poisson}\left(B_{ij}^t e^{s_B(1-V_{ij}^t/n_B^*)}\right), \quad V_{ij}^{t+1} = \text{Poisson}\left(V_{ij}^t e^{s_V(B_{ij}^t/n_B^*-1)}\right). \quad (\text{II1})$$

In the limit of strong HGT and  $s_B \sim s_V \ll 1$ , we can write eqs. (III1) into continuous equations, identical to eqs. (1) in the main text.

---

### Algorithm 1 Stochastic clone-based algorithm

---

- 1: Set model parameters  $L, s_B, s_V, r_B, r_V, N_B$  and  $N_V$ .
  - 2: Initialize the population size  $B_{ij}(t=0), V_{ij}(t=0)$  for each strain (genotype) with  $n_B^*$  and  $n_V^*$ , respectively.
  - 3: **for**  $t$  in  $1 : T$  **do**
  - 4:   **Selection process:**
  - 5:   Each host strain replicates itself following a Poisson distribution with the rates  $B_{ij}^t e^{s_B(1-V_{ij}^t/n_B^*)-\gamma \log \frac{\bar{N}_B}{N_B}}$ , where  $\bar{N}_B = \sum_{i < j} B_{ij} e^{s_V(1-V_{ij}^t/n_B^*)}$ . The term  $\gamma \log \frac{\bar{N}_B}{N_B}$  works as a regulator to constrain the total population approximately equal to  $N$  [43]. We set  $\gamma = 0$  for no population constraint and  $\gamma = 2$  for the hard constraint.
  - 6:   The phage replication follows a similar procedure.
  - 7:   **Horizontal Gene transfer process:**
  - 8:   Randomly select  $r_B N_B$  individuals from hosts and  $r_V N_V$  individuals from the phage.
  - 9:   For the **host-host** HGT case, then randomly select another  $r_B N_B$  genes from the hosts and replace one random gene from each of the selected  $r_B N_B$  host individuals with the selected genes. The **phage-phage** and **phage-host** cases follow similar procedures.
  - 10:   The **mean field approximation** case is equivalent to random mutations. To simulate this, we randomly mutate the selected genotype to an arbitrary genotype.
  - 11:   Add the  $r_B N_B$  new hosts and  $r_V N_V$  new phage back to the pool.
  - 12: **end for**
- 

All simulations are done with Julia. The codes are available on GitHub at <https://github.com/Wenping-Cui/GeneTransfer>.

## III: Canonical ensemble and Gamma distribution ansatz

In the deterministic limit, the antisymmetric Lotka-Volterra model for one host-phage pair has the following conserved quantity, i.e., the Lyapunov function:

$$E = (B - n_G^* \log \frac{B}{n_G^*}) + (V - n_G^* \log \frac{V}{n_G^*}), \quad (\text{III1})$$

where the superscript \* denotes the steady state.

Our system consists of many host-phage pairs coupled by gene exchange processes. Employing the idea of the canonical ensemble for interacting Lotka-Volterra systems [37], the total Lyapunov function can be written as

$$E_{tot} = \sum_i (B_i + V_i - n_G^* \log \frac{B_i}{n_G^*} - n_G^* \log \frac{V_i}{n_G^*}). \quad (\text{III2})$$

When all genes coexist for a long time, we may assume it is in *thermal equilibrium* and  $E_{tot}$  is conserved. It has been shown that the phase space has a unit of  $\log B_i \log V_i$  to secure Liouville's theorem [36, 37]; thus, we can derive the Boltzmann distribution from the principle of maximum entropy:

$$\rho(B, V) d\log B d\log V \propto e^{-(B+V - n_G^* \log \frac{B}{n_G^*} - n_G^* \log \frac{V}{n_G^*})/\Theta} d\log B d\log V, \quad (\text{III3})$$

where  $\Theta$  plays the role of an effective temperature. From the above expression, we can treat the host and phage abundance distributions as independent and identical. We use  $n_G$  to represent either the host or phage abundances and obtain

$$\rho(n_G) \propto \left( \frac{n_G}{n_G^*} \right)^{n_G^*/\Theta} n_G^{-1} e^{-n_G/\Theta}. \quad (\text{III4})$$

After normalization, this is equivalent to the *Gamma distribution*

$$\rho(n_G) = \text{Gamma}(n_G^*, \Theta) = \frac{n_G^{n_G^*/\Theta - 1} e^{-n_G/\Theta}}{\Theta^{n_G^*/\Theta} \Gamma(\frac{n_G^*}{\Theta})}, \quad (\text{III5})$$

where  $\Theta$  is an unknown variable determined by system properties but can be evaluated numerically through

$$\Theta = \langle (n_G - n_G^*)^2 \rangle / n_G^*, \quad (\text{III6})$$

where the average  $\langle \dots \rangle$  is taken over the whole time series in the thermodynamic equilibrium phase with all strains surviving.

### 1. Surviving fraction

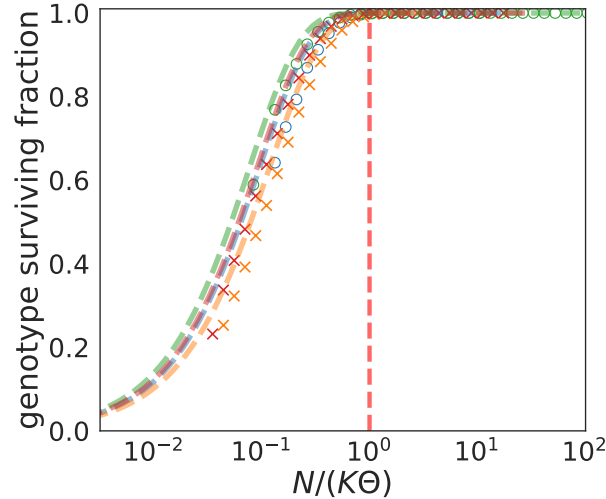


FIG. S1. Average surviving fraction of all genotypes over the whole time series. The red dashed line is  $N/(K\Theta) = 1$

We can estimate the average surviving fraction of all possible genotype over the time series by integrating the Gamma distribution from the natural cut-off 1 to infinity, yielding

$$f_s = \int_1^{+\infty} \frac{n_G^{n_G^*/\Theta - 1} e^{-n_G/\Theta}}{\Theta^{n_G^*/\Theta} \Gamma(\frac{n_G^*}{\Theta})} dn_G = \Gamma\left(\frac{N}{K\Theta}, \frac{1}{\Theta}\right) / \Gamma\left(\frac{N}{K\Theta}\right). \quad (\text{III7})$$

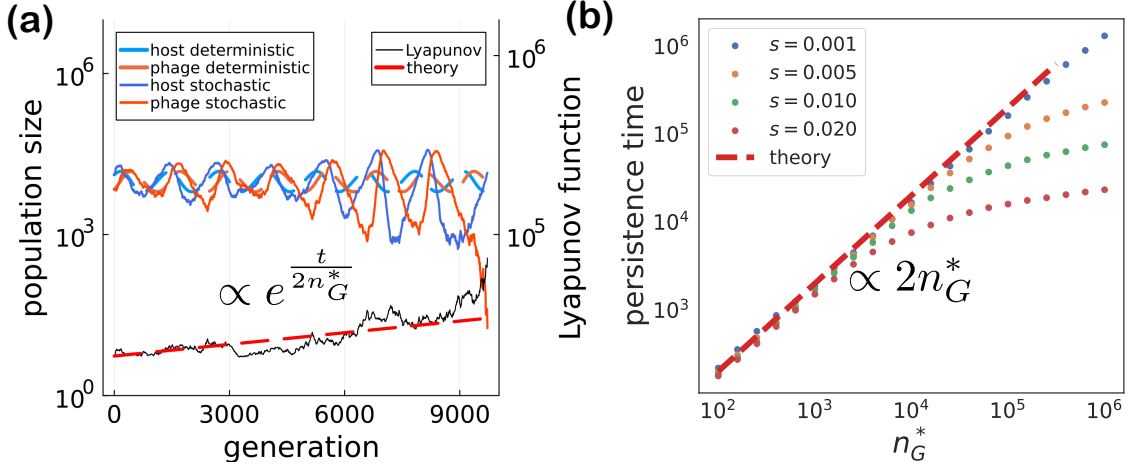


FIG. S2. Left  $y$  axis: deterministic and stochastic dynamics of one single pair of the host-phage system. Right  $y$  axis: the corresponding Lyapunov function and the theoretical prediction. The steady state for the phage and host is  $n_G^* = 10^4$ , and the intrinsic growth/death rate is  $s = 5 \times 10^{-3}$ ; (b) Persistence time for different  $n_G^*$  and  $s$ . The data points are averaged over 1000 trials of simulation.

We would like to note that here  $\Gamma\left(\frac{N}{K\Theta}, \frac{1}{\Theta}\right)$  is the incomplete gamma function to avoid confusion with the Gamma distribution notation in the main text. Fig. S1 shows eq. (III7) matches remarkably well with numerical simulation. Additionally, it reveals that the fraction of surviving genotypes begins to rapidly decline from 1 when the rate of the power law component of the Gamma distribution falls below 1, signifying the onset of Regime II, where genotype extinctions occur.

#### IV: Stochastic LV model without horizontal gene transfer

In the deterministic limit, the host and phage dynamics form a prey-predator oscillator that can oscillate forever. When the population size is finite, the stochasticity will drive the oscillation amplitude to increase until either the host or the phage goes extinct, as shown in Fig. S2a. In this section, we will derive the scaling of the extinction time.

When the gene exchange rate is negligible compared the typical selection rate,

$$r \ll s(1 - V/n_G^*) \sim s(B/n_G^* - 1) \ll 1, \quad (\text{IV1})$$

we no longer consider HGT. Assuming the fitnesses for the host and phage,  $s(1 - V/n_G^*)$  and  $s(B/n_G^* - 1)$ , are much smaller than 1, we can consider the stochastic LV equations

$$\begin{aligned} \frac{dB}{dt} &= sB(1 - V/n_G^*) + \sqrt{B}\eta_B, \\ \frac{dV}{dt} &= sV(B/n_G^* - 1) + \sqrt{V}\eta_V. \end{aligned} \quad (\text{IV2})$$

where  $\eta_B$  and  $\eta_V$  are white noises with  $\langle \eta_B(t) \rangle = \langle \eta_V(t) \rangle = 0$ ,  $\langle \eta_B(t)\eta_V(t') \rangle = 0$ ,  $\langle \eta_B(t)\eta_B(t') \rangle = \delta(t - t')$ , and  $\langle \eta_V(t)\eta_V(t') \rangle = \delta(t - t')$ .

Instead of studying the two-dimensional nonlinear LV dynamics, we can study its stability through the Lyapunov function [30] given by eq. (III1). Substituting eq. (III1) into the deterministic part of eqs. (IV2) shows that the Lyapunov function is conserved in the deterministic case, corresponding to a stable oscillator.

For the stochastic LV model, we can apply Itô's lemma [39],

$$\begin{aligned} dE &= \left( \frac{\partial E}{\partial B} \frac{dB}{dt} + \frac{\partial E}{\partial V} \frac{dV}{dt} \right) dt + \frac{1}{2} \left( \frac{\partial^2 E}{\partial B^2} B + \frac{\partial^2 E}{\partial V^2} V \right) dt + \sqrt{B} \frac{\partial E}{\partial B} d\eta_B + \sqrt{V} \frac{\partial E}{\partial V} d\eta_V \\ &= n_G^* \left( \frac{1}{2B} + \frac{1}{2V} \right) dt + \sqrt{\frac{(B - n_G^*)^2}{B} + \frac{(V - n_G^*)^2}{V}} d\eta \\ &= \frac{n_G^* (E + n_G^* \log \frac{B}{n_G^*} + n_G^* \log \frac{V}{n_G^*})}{2BV} dt + \sqrt{\frac{(B - n_G^*)^2}{B} + \frac{(V - n_G^*)^2}{V}} d\eta \end{aligned} \quad (\text{IV3})$$



We can apply a linear-noise approximation around the steady state to approximate it as

$$dE \approx \left[ \frac{E}{2n_G^*} - \frac{E(\Delta V + \Delta B)}{2(n_G^*)^2} + \frac{\Delta V + \Delta B}{2n_G^*} \right] dt + \sqrt{\frac{\Delta B^2 + \Delta V^2}{n_G^*}} d\eta. \quad (\text{IV4})$$

where  $B = n_G^* + \Delta B$  and  $V = n_G^* + \Delta V$ . In the limit  $n_G^* \gg \Delta V, \Delta B$ , we can keep the zeroth order, and the Lyapunov function grows exponentially with time:

$$E(t) \approx E(0)e^{\frac{t}{2n_G^*}}. \quad (\text{IV5})$$

We do not know the threshold of the Lyapunov function when the oscillator becomes unstable. However, from eq. (IV5), we can roughly estimate the typical persistence time of the oscillator to be about  $2n_G^*$ .

Fig. S2a shows one simulation trial with the initial condition around the steady state, and the Lyapunov function grows approximately like eq. (IV5). Fig. S2b compares the average persistence time with our theory, and  $2n_G^*$  is a good estimation when the average clone size is below  $10^5$ . This is surprising because our result is based on the linear-noise approximation, which is no longer valid when the system is far from the steady state. Luckily, the amplitude of the oscillator increases dramatically after the linear-noise approximation fails, so our approximation is not bad.

## V: Regime III: stochastic oscillation with high HGT rates

### 1. Stochastic Lotka-Volterra equations with HGT

In this regime, the HGT rate is comparable to or larger than the fitness, i.e.,

$$s(-V/n_G^* + 1) \sim s(B/n_G^* - 1) \lesssim r \ll 1, \quad (\text{V1})$$

but both are still small compared with 1. We can write down the approximated Langevin equations:

$$\begin{aligned} \frac{dB}{dt} &= sB(-V/n_G^* + 1) + rn_G^* + \sqrt{B}\eta_B, \\ \frac{dV}{dt} &= sV(B/n_G^* - 1) + rn_G^* + \sqrt{V}\eta_V. \end{aligned} \quad (\text{V2})$$

The first term is the ordinary Lotka-Volterra dynamics. For the second term, we assume that the HGT process uniformly samples over the whole genotype space. This suggests HGT plays a similar role to migrations [31, 52, 53]. The third term comes from the demographic noise.

Applying Itô's lemma [39], the stochastic differential equation of eq. (III1) becomes

$$\begin{aligned} dE &= \left( \frac{\partial E}{\partial B} \frac{dB}{dt} + \frac{\partial E}{\partial V} \frac{dV}{dt} \right) dt + \frac{1}{2} \left( \frac{\partial^2 E}{\partial B^2} B + \frac{\partial^2 E}{\partial V^2} V \right) dt + \sqrt{B} \frac{\partial E}{\partial B} d\eta_B + \sqrt{V} \frac{\partial E}{\partial V} d\eta_V \\ &= \left( \frac{n_G^*}{2B} + \frac{n_G^*}{2V} + r \frac{n_G^*(B - n_G^*)}{B} + r \frac{n_G^*(V - n_G^*)}{V} \right) dt + \sqrt{\frac{(B - n_G^*)^2}{B} + \frac{(V - n_G^*)^2}{V}} d\eta. \end{aligned} \quad (\text{V3})$$

### 2. Self-consistency relations

#### a. Solution of $\Theta$ and critical point

In this regime, we hope that the time average of the Lyapunov function does not change. We then evaluate the drift part averaged with the canonical ensemble

$$\int \rho(B)\rho(V) \left( \frac{n_G^*}{2B} + \frac{n_G^*}{2V} + r \frac{n_G^*(B - n_G^*)}{B} + r \frac{n_G^*(V - n_G^*)}{V} \right) dBdV = \frac{n_G^*}{(n_G^* - \Theta)} - \frac{2rn_G^*\Theta}{n_G^* - \Theta} = 0. \quad (\text{V4})$$

where  $\rho(B), \rho(V)$  are Gamma distributions defined in eq. (III4). The self-consistency relation gives

$$\Theta = \begin{cases} \frac{1}{2r}, & 2rn_G^* - 1 > 0, \\ \text{no solution}, & 2rn_G^* - 1 \leq 0. \end{cases} \quad (\text{V5})$$

Our analytical solution suggests there is a transition at  $2rn_G^* = 1$ . The underlying reason is that the left tail of genotype Gamma distribution follows a power law with the exponent  $2rn_G^* - 1$ . When the power exponent is below zero,  $\rho(n_G)$  diverges at  $n_G \rightarrow 0$ , suggesting the phage and host can go extinct, and only a fraction of genotypes are present in the system. Thus, the critical transition between Regime II and III happens at

$$r_c^G = \frac{1}{2n_G^*} = \frac{K}{2N}. \quad (\text{V6})$$

*b. An alternative explanation from LV dynamics*

We can see HGT processes help stabilize the system in the deterministic term in eq. (V3). We want to ensure that the deterministic term is negative when the oscillation amplitude is large. Regarding the symmetry between  $B$  and  $V$ , we only consider the case  $B \ll n_G^*$  and  $V \gg n_G^*$  and ignore the phage part in the term. Then we obtain the stability condition:  $\frac{n_G^*}{2B} - r\frac{(n_G^*)^2}{B} < 0$ , yielding

$$2rn_G^* - 1 > 0, \quad (\text{V7})$$

which provides an alternative view of the critical transition at  $r_c^G$ , suggesting the predictions of  $r_c^G$  from canonical ensemble and stochastic LV dynamics are consistent with each other.

## VI: Regime II: boom-bust cycles with low HGT rates

When the HGT rate is weak, some phage or host genotypes go extinct and take a long time to return to the ecosystem. In this regime, there are boom-bust cycles as in Fig. 1b, and the continuous stochastic Lotka-Volterra equation is no longer valid. Most of the time, the phage and host barely interact with each other, so we can apply a *Branching Process* analysis to this regime.

The rising host has an approximately constant fitness  $s$  as its corresponding phage has a small population size. Fig. S3a shows that after the rising host gets established, it will grow exponentially with rate  $s$  until the corresponding phage gets established.

### 1. Establishment (fixation) probability in a changing environment

Assuming the host starts to grow exponentially at  $t = 0$  with some established population size  $n_0$ , the phage's fitness  $x$  follows

$$x(t) = s \left( \frac{n_0}{n_G^*} e^{st} - 1 \right). \quad (\text{VI1})$$

Eq. (VI1) shows the phage only has a positive fitness after the host exceeds the mean population size, and thus we are only interested in the time after the host population size exceeds  $n_G^*$ . We set the time when the host population size equals  $n_G^*$  as zero. We want to answer the question: after a duration  $\tau$ , there are corresponding phages reborn from HGT; what is the probability that they get established? This can be solved by a branching process in a changing environment [44] (also see the scheme at Fig. S3c).

We rewrite the phage's fitness into

$$x(\tau) = s(e^{s\tau} - 1), \quad (\text{VI2})$$

where  $\tau = 0$ , as we defined, is when the host population exceeds its mean abundance.

We assume the extinction probability after  $t$  generations for a phage sampled at a given time  $\tau$  follows a branching process with two offspring:

$$w(t|\tau) = [1 - (x(\tau) + 2)\Delta t]w(t - \Delta t|\tau + \Delta t) + \Delta t + (1 + x(\tau))\Delta t w(t - \Delta t|\tau + \Delta t)^2. \quad (\text{VI3})$$

It is easier to use the variable  $x$  instead of  $\tau$ , where  $x$  is the fitness at time  $\tau$ ,

$$w(t|x) = [1 - (x + 2)\Delta t]w(t - \Delta t, x + s(x + s)\Delta t) + \Delta t + (1 + x)\Delta t w(t - \Delta t, x + s(x + s)\Delta t)^2. \quad (\text{VI4})$$

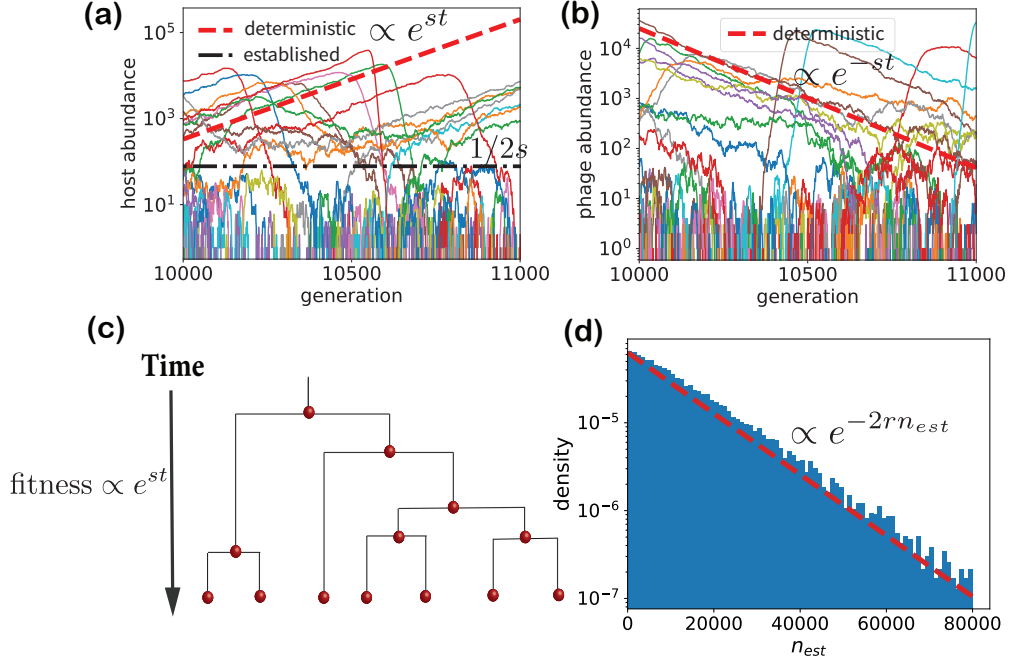


FIG. S3. **(a)** A snapshot of multiple-host population dynamics. The black dotted-dash line is the typical established population size  $\frac{1}{2s}$  as a boundary between stochastic fluctuation and deterministic growth  $\propto e^{st}$  (the red dashed line). **(b)** A snapshot of multiple-phage population dynamics. The red dashed line shows the phage abundance almost decreased  $\propto e^{-st}$  deterministically after dramatically booming. **(c)** A schematic illustrating a branching process of one strain of phages with its fitness increasing exponentially in time as its susceptible host follows exponential growth. **(d)** The distribution of the host abundance at the moment when the phage gets established and starts booming follows our theoretical prediction: an exponential distribution  $\propto e^{-2rn_{est}}$ .

In the continuum limit,

$$\frac{\partial w(t|x)}{\partial t} - s(x+s) \frac{\partial w(t|x)}{\partial x} = 1 - (x+2)w(t,x) + (1+x)w(t|x)^2. \quad (\text{VI5})$$

We can rewrite the above equation into the survival probability  $\phi(t,x) = 1 - w(t|x)$ ,

$$\frac{\partial \phi(t,x)}{\partial t} - s(x+s) \frac{\partial \phi(t,x)}{\partial x} = x\phi(t,x) - (1+x)\phi(t,x)^2. \quad (\text{VI6})$$

We are interested in the establishment probability, which is equivalent to the survival probability in the long, but finite, time limit. In this limit,  $\phi(t,x)$  is not sensitive to time and can be written as  $\phi(x)$ ,

$$-s(x+s) \frac{\partial \phi(x)}{\partial x} = x\phi(x) - (1+x)\phi(x)^2. \quad (\text{VI7})$$

In the limit of  $sx \ll 1$  and  $x \gg s$ ,

$$\phi(x) \approx \frac{x}{1+x} \approx \frac{se^{s\tau}}{1+se^{s\tau}}. \quad (\text{VI8})$$

In deriving the survival probability, we assumed there were two offspring in the birth-death process. Our simulation uses a Poisson process to sample the number of offspring, (see Sec. X 2), which contributes a factor of 2. After correction, it becomes

$$\phi(\tau) \approx \frac{2se^{s\tau}}{1+2se^{s\tau}}. \quad (\text{VI9})$$

## 2. Sampling from HGT

We assume the phage sampled from HGT follows a Poisson process with a constant event rate  $\frac{r}{K}$  per individual per generation per strain. In principle, the HGT process depends on the time-varying gene abundance. However, Fig. S9 shows the gene dynamics, as the sum of  $L - 1$  genotype dynamics, have much smaller fluctuations and are also weakly correlated with the genotype dynamics, so we can take the average value and assume the event rate is a constant. The probability for sampling  $n$  phages of a specific genotype is given as

$$P(n) = \frac{e^{-\frac{rN}{K}}}{n!} \left( \frac{rN}{K} \right)^n. \quad (\text{VI10})$$

We must consider that the establishment probability varies at different generations. The probability of  $k$  established phages born at generation  $\tau$  is given by

$$\begin{aligned} P(k, \tau) &= \sum_{n=k}^{\infty} \frac{e^{-\frac{rN}{K}}}{n!} \left( \frac{rN}{K} \right)^n \binom{n}{k} \phi(\tau)^k (1 - \phi(\tau))^{n-k} \\ &= \frac{e^{-\frac{rN\phi(t)}{K}}}{k!} \left( \frac{rN\phi(t)}{K} \right)^k \sum_{n=k}^{\infty} \frac{e^{-\frac{rN}{K} + \frac{rN\phi(t)}{K}}}{(n-k)!} \left( \frac{rN}{K} - \frac{rN\phi(t)}{K} \right)^{n-k} \\ &= \frac{e^{-\frac{rN\phi(t)}{K}}}{k!} \left( \frac{rN\phi(t)}{K} \right)^k, \end{aligned} \quad (\text{VI11})$$

which is an inhomogeneous Poisson distribution [42, 54].

We are interested in when the first phage becomes established between  $T$  and  $T + \Delta T$ . In our simulation, we set  $\Delta T = 1$  and the survival probability after exactly  $T$  generations follows an exponential distribution,

$$P(T) = \frac{rN}{K} \phi(T) e^{-\frac{rN}{K} \int_0^T \phi(\tau) d\tau}. \quad (\text{VI12})$$

We can evaluate its exponential part by

$$\frac{rN}{K} \int_0^T \phi(\tau) d\tau = \frac{rN}{K} \int_0^T \frac{2se^{s\tau}}{1 + 2se^{s\tau}} d\tau = \frac{rN}{Ks} \log \left( \frac{1 + 2se^{sT}}{1 + 2s} \right) \approx 2rn_G^* e^{sT}. \quad (\text{VI13})$$

Here we employ the fact that a typical establishment time  $T$  obeys  $se^{sT} \ll 1$  because the phage fitness is small.

We can write down its approximated probability distribution and consider the normalization

$$P(T) \approx 2srn_G^* e^{2rn_G^* + sT - 2rn_G^* e^{sT}}. \quad (\text{VI14})$$

Interestingly, this is the half-truncated *Gumbel distribution*.

We are interested in the host population size when the first phage gets established; it follows (see Sec. IX)

$$Q(n_G) = \frac{1}{sn_G} P\left(\frac{1}{s} \log \frac{n_G}{n_G^*}\right) = 2re^{-2r(n_G - n_G^*)}, \quad n_G^* \leq n_G < \infty. \quad (\text{VI15})$$

We examine the above equation with numerical simulations, and it fits well as shown in Fig. S3d.

## 3. Consistency with canonical ensemble

To be self-consistent with the exponential tail of the Gamma distribution in eq. (III5), the effective temperature is given by

$$\Theta \approx \frac{1}{2r}. \quad (\text{VI16})$$

A question is raised as to why eq. (VI15) follows the exponential distribution instead of the Gamma distribution. This is because we draw the histogram from the whole time series, which can be viewed as the sum of many independent and identical exponential distributions, naturally yielding the Gamma distribution. Our analysis matches well with simulation, as shown in Fig. 3 in the main text.



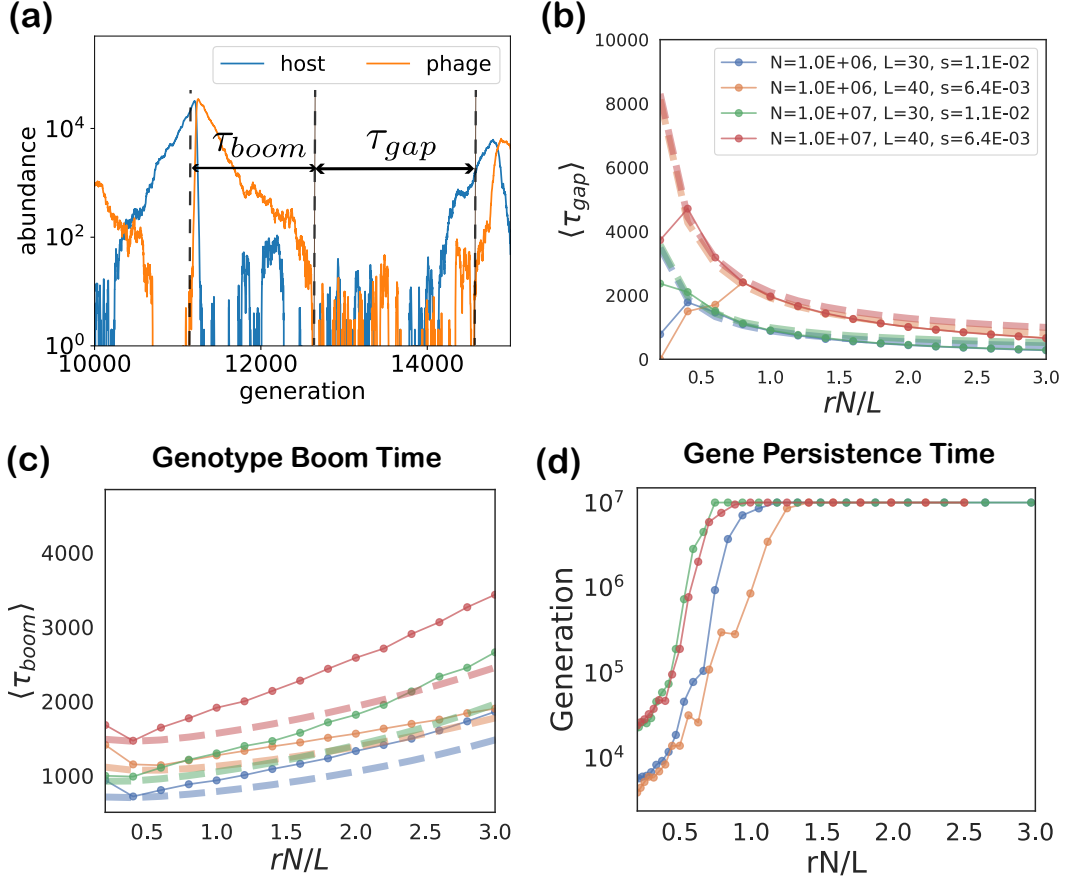


FIG. S4. **(a)** Scheme for the definition of the gap time  $\tau_{gap}$  between two booms of phage and the phage booming time  $\tau_{boom}$  in the boom-bust dynamics. **(b, c)** Comparison of the averaged  $\tau_{gap}$  and  $\tau_{boom}$  from simulation and our theoretical predictions (dashed lines). **(d)** Gene survival time for different  $L$  and  $N$  with a simulation time limit of  $10^7$  generations.

#### 4. Booming duration and time gap between consecutive booms

It is interesting to investigate properties of the boom-bust cycles: the boom duration  $\tau_{boom}$  as the time elapsed when the host gets established ( $n_{est} \sim \frac{1}{2s}$ ), reaches the peak ( $n_G \sim \frac{1}{2r}$ ) and then dies out,  $n_G = 0$ ; and the gap time between two peaks:  $\tau_{gap}$ , shown in Fig. S4a. Because of time-reversal symmetry (perfect anti-symmetry),  $\tau_{gap}$  and  $\tau_{boom}$  are identical for phages and hosts.

Considering the host, we can estimate the booming duration by the following equation:

$$\tau_{boom} = \frac{1}{s} \log \frac{s}{r} + \frac{4rn_G^*}{s(1 - 2rn_G^*)} \log \frac{1}{2r}. \quad (\text{VI17})$$

The first term describes the exponential growth time from the established population size to the typical boom size. The second term describes two sequential processes: the phage reaches its boom size, and then, the host drops to zero. We assume the two processes have the same typical time scale, contributing a factor of 2.

$\tau_{gap}$ , the time between when the host/phage goes extinct and when it gets established, can be written as

$$\tau_{gap} = \frac{1}{2s} \left( \frac{1}{rn_G^*} + \log \frac{s}{r} \right). \quad (\text{VI18})$$

The first term describes the typical time for a host with a survival probability  $2s$  and a HGT rate  $rN/K$  to get established [42]. The second term results from the correction that the host boom is always followed by the phage boom, and the host cannot get established when the phage is in the boom phase.

In the simulation,  $\tau_{boom}$  for the host is underestimated. This is because the host has a higher chance to undergo continuous booms after the phage dies, but the phage dies immediately after the host dies. In Fig. S4bc, we show our analytical estimation agrees well with the simulation.

Fig. S4d gives a higher resolution of  $r$  near the transition between Regime I and II.  $rN/L = 1$  is the critical boundary given by eqs. (6) in the main text. It shows when passing  $r_c^g$ , i.e.,  $rN/L > 1$ , the strain boom time does not vary much, but the gene persistence time can increase dramatically, much faster than exponential growth.

### 5. Mean population size without the population size constraint

In Regime III, the prey-predator oscillator oscillates around the steady state  $n_G^*$ , causing the mean population size over the time series to also be  $n_G^*$ . However, in the boom-bust dynamics, for instance, the host undergoes exponential growth and catastrophic recession, which does not have a steady state. We choose a hard constraint for the total population size and hence the average must be equal to  $n_G^*$ .

The reader may be curious about the average clone size of each strain if we remove the hard constraint about the total population size. The gap period between two booms is given by

$$\tau_{gap} \approx \frac{1}{2srn_G^*}, \quad (\text{VI19})$$

which leads to

$$\langle n \rangle = \frac{\int_0^{\frac{1}{s} \log \frac{s}{r}} dt \frac{1}{2s} e^{st}}{\frac{1}{s} \log \frac{s}{r} + \tau_{gap}} = \frac{\frac{1}{2sr} - \frac{1}{2s^2}}{\frac{1}{s} \log \frac{s}{r} + \frac{1}{2srn_G^*}} \approx n_G^*. \quad (\text{VI20})$$

The above equation is a rough estimation. It needs careful treatment when the phages and hosts are not perfectly anti-symmetric.

## VII: Different mechanisms of horizontal gene transfer

For the gene abundance distribution, it is helpful to normalize the population size to its fraction:

$$\begin{aligned} \frac{dP_{ij}}{dt} &= sK P_{ij} \left( \frac{1}{K} - Q_{ij} \right) + J_{ij}^P + \sqrt{\frac{P_{ij}}{N}} \eta_P, \\ \frac{dQ_{ij}}{dt} &= sK Q_{ij} \left( P_{ij} - \frac{1}{K} \right) + J_{ij}^Q + \sqrt{\frac{Q_{ij}}{N}} \eta_Q, \end{aligned} \quad (\text{VII1})$$

where  $P_{ij} = \frac{1}{N} B_{ij}$ ,  $Q_{ij} = \frac{1}{N} V_{ij}$  are the fraction of host/phage genotypes carrying genes  $i, j$  so that the average of the off-diagonal elements  $\langle P_{ij} \rangle = \langle Q_{ij} \rangle = 1/K$ . We set  $P_{ii} = Q_{ii} = 0$ ,  $P_{ij} = P_{ji}$ , and  $Q_{ij} = Q_{ji}$  as each individual carries two different genes, and the order of genes does not affect the genotype. In other words,  $P_{ij}$  and  $Q_{ij}$  are symmetric matrices with diagonal elements equal to zero.  $J_{ij}^X$ , represents the influx of clones for a specific genotype  $X_{ij}$ , and their forms depend on the detailed HGT processes.

We would like to emphasize that the scaling of  $\theta$  and  $\Theta$  is also changed after normalization of the population size. As a result, we define  $\bar{\theta}$  and  $\bar{\Theta}$  for the normalized genotype and gene abundances, which obey

$$\theta = N\bar{\theta}, \quad \Theta = N\bar{\Theta}.$$

### 1. Ideal mean-field case

In this ideal case, we assume the rate of genotype generation is constant so that the clone influx is also constant. The dynamics are

$$\begin{aligned} \frac{dP_{ij}}{dt} &= sK P_{ij} \left( \frac{1}{K} - Q_{ij} \right) + \frac{r}{K} + \sqrt{\frac{P_{ij}}{N}} \eta_P, \\ \frac{dQ_{ij}}{dt} &= sK Q_{ij} \left( P_{ij} - \frac{1}{K} \right) + \frac{r}{K} + \sqrt{\frac{Q_{ij}}{N}} \eta_Q. \end{aligned} \quad (\text{VII2})$$

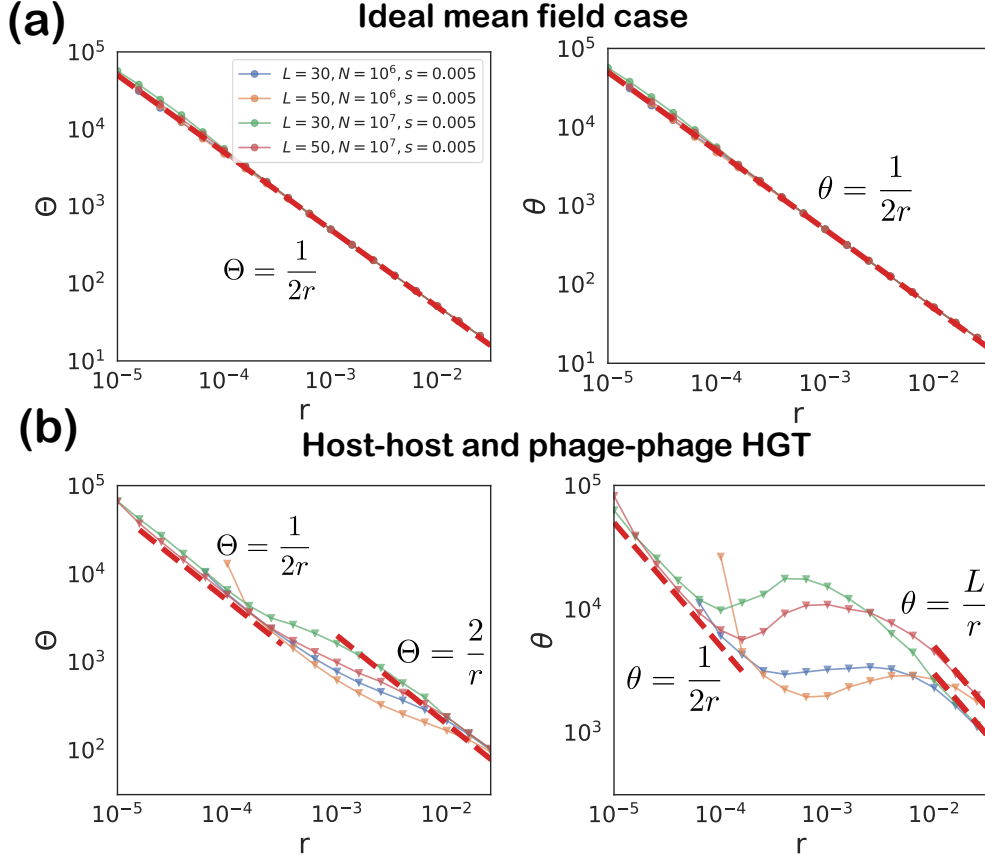


FIG. S5. Effective genotype and gene temperature for (a) the ideal mean field case, (b) host-host and phage-phage HGT processes. The red dashed lines are theoretical predictions.

We are interested in the marginal probability of genes:  $p_i = \sum_j P_{ij}$  and  $q_i = \sum_j Q_{ij}$ . We would like to note that

$$\sum_i p_i = \sum_i q_i = 2, \quad (\text{VII3})$$

as each individual carries two genes, so it is not normalized. The influx for one specific gene is

$$j_i^p = \sum_j J_{ij}^p = \frac{2r}{L}, \quad j_i^q = \sum_j J_{ij}^q = \frac{2r}{L}, \quad (\text{VII4})$$

which are also constant in this ideal case.

The dynamics of  $p_i, q_i$  become

$$\begin{aligned} \frac{dp_i}{dt} &\approx sp_i - sK \sum_j P_{ij} Q_{ij} + \frac{2r}{L} + \sqrt{\frac{p_i}{N}} \eta_p, \\ \frac{dq_i}{dt} &\approx sK \sum_j P_{ij} Q_{ij} - sq_i + \frac{2r}{L} + \sqrt{\frac{q_i}{N}} \eta_q. \end{aligned} \quad (\text{VII5})$$

We can evaluate the second term,  $\sum_j P_{ij} Q_{ij}$ , by assuming  $P_{ij}$  and  $Q_{ij}$  are weakly correlated:

$$\sum_j P_{ij} Q_{ij} \approx \frac{1}{L} p_i q_i. \quad (\text{VII6})$$

Combining the above relations, we have

$$\begin{aligned}\frac{dp_i}{dt} &\approx \frac{Ls}{2}p_i \left( \frac{2}{L} - q_i \right) + \frac{2r}{L} + \sqrt{\frac{p_i}{N}}\eta_p, \\ \frac{dq_i}{dt} &\approx \frac{Ls}{2}q_i \left( p_i - \frac{2}{L} \right) + \frac{2r}{L} + \sqrt{\frac{q_i}{N}}\eta_q.\end{aligned}\tag{VII7}$$

Similar to eq. (V3), we can calculate the effective temperature of the Gamma distribution for  $p_i$ ,  $q_i$ , and then rescale back to its population size. This gives

$$\theta = \frac{1}{2r}.\tag{VII8}$$

## 2. Host-host and phage-host HGT

In this case, we take the phage-host and host-host HGT into consideration, and the inflow HGT terms in eq. (VIII1) become

$$\begin{aligned}J_{ij}^p &= \frac{r}{4} \sum_{j' \neq j} P_{ij'} p_j + \frac{r}{4} \sum_{i' \neq i} P_{i'j} p_i + \frac{r}{2} P_{ij} (p_i + p_j) \\ &= \frac{r}{4} (p_i - P_{ij}) p_j + \frac{r}{4} (p_j - P_{ij}) p_i + \frac{r}{2} P_{ij} (p_i + p_j) \\ &= \frac{r}{2} p_i p_j + \frac{r}{4} P_{ij} (p_i + p_j).\end{aligned}$$

Looking at the the first line of the above equation,  $rP_{ij'}p_j/2$  and  $rP_{i'j}p_i/2$  describe the probability that one strain with one site difference, picks up gene  $i$  and transforms into genotype  $ij$ , noting that  $p_i/2$  results from the normalization of  $p_i$ . It is then divided by another factor of 2 since we do not count the order of two genes.  $rP_{ij}(p_i/2 + p_j/2)$  describes the probability that one genotype stays the same after the HGT. Similarly, we have

$$J_{ij}^q = \frac{r}{4} \sum_{j'} Q_{ij'} p_j + \frac{r}{4} \sum_{i'} Q_{i'j} p_i + \frac{r}{2} Q_{ij} (p_i + p_j) = \frac{r}{4} q_i p_j + \frac{r}{4} q_j p_i + \frac{r}{4} Q_{ij} (p_i + p_j).$$

We can write the gene dynamics as

$$\begin{aligned}\frac{dp_i}{dt} &= \frac{Ls}{2}p_i \left( \frac{2}{L} - q_i \right) + \frac{r}{2}p_i \sum_j p_j + \frac{r}{4}p_i^2 + \frac{r}{4} \sum_j P_{ij} p_j + \sqrt{\frac{p_i}{N}}\eta_p, \\ \frac{dq_i}{dt} &= \frac{Ls}{2}q_i \left( p_i - \frac{2}{L} \right) + \frac{r}{4}q_i \sum_j p_j + \frac{r}{4}p_i \sum_j q_j + \frac{r}{4}p_i q_i + \frac{r}{4} \sum_j Q_{ij} p_j + \sqrt{\frac{q_i}{N}}\eta_q.\end{aligned}\tag{VII9}$$

Utilizing  $\sum_{j \neq i} p_j = 2 - p_i$  and  $\sum_{j \neq i} q_j = 2 - q_i$ , it can be reduced to

$$\begin{aligned}\frac{dp_i}{dt} &= \frac{Ls}{2}p_i \left( \frac{2}{L} - q_i \right) + \frac{r}{4} \sum_j P_{ij} p_j - \frac{r}{4}p_i^2 + rp_i + \sqrt{\frac{p_i}{N}}\eta_p, \\ \frac{dq_i}{dt} &= \frac{Ls}{2}q_i \left( p_i - \frac{2}{L} \right) + \frac{r}{2} (p_i - q_i) + \frac{r}{4} \sum_j Q_{ij} p_j - \frac{r}{4}p_i q_i + rq_i + \sqrt{\frac{q_i}{N}}\eta_q.\end{aligned}\tag{VII10}$$

### a. Decoupling of gene and genotype dynamics

Fig. S9 suggests the different gene and genotype dynamics are weakly correlated. Hence we can average the gene dynamics out:

$$\sum_j P_{ij} p_j \approx \frac{2}{L} p_i, \quad \sum_j Q_{ij} p_j \approx \frac{2}{L} q_i.\tag{VII11}$$



The mean-field gene dynamics become

$$\begin{aligned}\frac{dp_i}{dt} &= \frac{Ls}{2} p_i \left( \frac{2}{L} - q_i \right) + \frac{r}{4} p_i \left( \frac{2}{L} - p_i \right) + r p_i + \sqrt{\frac{p_i}{N}} \eta_p, \\ \frac{dq_i}{dt} &= \frac{Ls}{2} q_i \left( p_i - \frac{2}{L} \right) + \frac{r}{2} (p_i - q_i) + \frac{r}{4} q_i \left( \frac{2}{L} - p_i \right) + r q_i + \sqrt{\frac{q_i}{N}} \eta_q.\end{aligned}\tag{VII12}$$

With  $p^* = q^* = \frac{2}{L}$ , similar to eq. (V3), we can write down the dynamics of the Lyapunov function for the gene dynamics as:

$$\begin{aligned}dE &= \left( \frac{p^*}{2Np_i} + \frac{p^*}{2Nq_i} - \frac{r}{4} (p_i - p^*)^2 - \frac{r}{2q_i} (q^* - q_i)^2 \right) dt \\ &\quad + \left( \frac{r}{2q_i} - \frac{r}{4} \right) (p_i - p^*) (q_i - q^*) dt + r(p_i - p^*) dt + r(q_i - q^*) dt + \sqrt{\frac{(p_i - p^*)^2}{Np_i} + \frac{(q_i - p^*)^2}{Nq_i}} d\eta.\end{aligned}\tag{VII13}$$

The self-consistency relation yields

$$\begin{aligned}&\int \rho(p_i) \rho(q_i) \left[ \frac{p^*}{2Np_i} + \frac{p^*}{2Nq_i} - \frac{r}{4} (p_i - p^*)^2 - \frac{r}{2q_i} (q^* - q_i)^2 \right] dq_i dp_i \\ &= p^* \left[ \frac{1}{N(p^* - \bar{\theta})} - \frac{r}{4} \bar{\theta} - \frac{r\bar{\theta}}{2(p^* - \bar{\theta})} \right] = 0.\end{aligned}\tag{VII14}$$

In the limit  $rN \gg 1$ , it gives

$$\theta = N\bar{\theta} = N \left[ \frac{L+1}{L} - \sqrt{\left( \frac{L+1}{L} \right)^2 - \frac{4}{rN}} \right] \approx \frac{2}{r}.\tag{VII15}$$

### 3. Host-host and phage-phage HGT

Similar to the phage-host HGT case, we can write down the mean-field gene dynamics as

$$\begin{aligned}\frac{dp_i}{dt} &= \frac{2s}{L} p_i \left( \frac{2}{L} - q_i \right) + \frac{r}{4} p_i \left( \frac{2}{L} - p_i \right) + r p_i + \sqrt{\frac{p_i}{N}} \eta_p, \\ \frac{dq_i}{dt} &= \frac{2s}{L} q_i \left( p_i - \frac{2}{L} \right) + \frac{r}{4} q_i \left( \frac{2}{L} - q_i \right) + r q_i + \sqrt{\frac{q_i}{N}} \eta_q.\end{aligned}\tag{VII16}$$

The dynamics of the Lyapunov function is

$$\begin{aligned}dE &= \left( \frac{p^*}{2Np_i} + \frac{q^*}{2Nq_i} - \frac{r}{4} (p_i - p^*)^2 - \frac{r}{4} (q_i - q^*)^2 \right) dt \\ &\quad + r(p_i - p^*) dt + r(q_i - q^*) dt + \sqrt{\frac{(p_i - p^*)^2}{Np_i} + \frac{(q_i - p^*)^2}{Nq_i}} d\eta.\end{aligned}\tag{VII17}$$

The self-consistency relation yields

$$\int \rho(p_i) \rho(q_i) \left[ \frac{p^*}{2Np_i} + \frac{q^*}{2Nq_i} - \frac{r}{4} (p_i - p^*)^2 - \frac{r}{4} (q_i - q^*)^2 \right] dq_i dp_i = \frac{p^*}{N(p^* - \bar{\theta})} - \frac{r}{2} p^* \bar{\theta} = 0,\tag{VII18}$$

which gives

$$\theta = N\bar{\theta} = N \left( \frac{1}{L} - \sqrt{\frac{1}{L^2} - \frac{2}{Nr}} \right) \approx \frac{L}{r}.\tag{VII19}$$

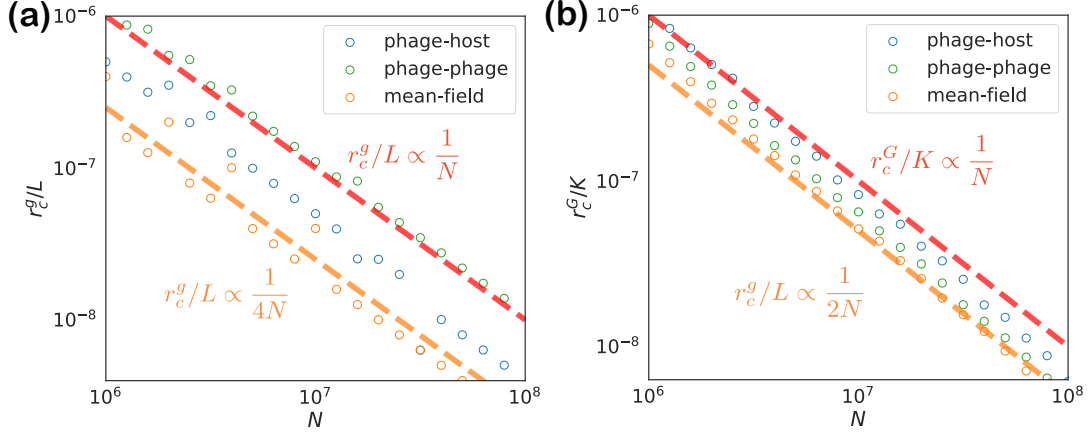


FIG. S6. Comparison of minimal HGT rates for (a) gene coexistence and (b) genotype coexistence for different types of HGT: host-host and phage-host HGT, host-host and phage-phage HGT. We also conduct simulations with constant rates of genotype generation from the mean-field approximation for comparison. As expected, our mean field theoretical prediction (the orange lines) matches perfectly with the simulation with constant rates of genotype generation from mean field estimation, but falls off with a factor within order 1 for the two different HGT processes (the red lines are theoretical predictions dropping the prefactor).

#### a. Effective genotype temperature

The above result shows the effective gene temperature is proportional to  $L$ , much larger than the phage-host case. This strong gene-gene correlation leads to a correction to  $\Theta$ , which is challenging to evaluate from the genotype dynamics as we can no longer decouple the gene and genotype dynamics.

Thanks to the quasi-linkage equilibrium in the strong HGT regime [38], we can approximate the genotype fraction by the product of its marginal gene fraction,  $P_{ij} \propto p_i p_j$ ,  $Q_{ij} \propto q_i q_j$  and obtain that  $P_{ij}, Q_{ij}$  follow a PDF:

$$\rho(x) = \frac{2x^{rN/L^2-1} K_0(2rN\sqrt{x}/L)}{(\frac{L}{rN})^{2rN/L^2} [\Gamma(rN/L^2)]^2}, \quad (\text{VII20})$$

where  $x$  represents either  $P_{ij}$  or  $Q_{ij}$ , and  $K_n$  is the modified Bessel function of the second kind. The above PDF has mean  $1/L^2$  and variance  $\frac{L^2+2Nr}{N^2L^2r^2}$ . Then we can use eq. (VII20) to roughly estimate  $\Theta$  for the Gamma distribution, which gives

$$\Theta \approx \frac{L^2 + 2Nr}{Nr^2} \approx \frac{2}{r}. \quad (\text{VII21})$$

## 4. Summary

We summarize the analytical results in Table I and show the comparison with numerical simulations in Fig. 4ab in the main text and Fig. S5. The scaling of  $\Theta$  and  $\theta$  shows different implementations of the HGT processes do not affect our criteria eqs. (7) much (see Fig. S6). We get the critical  $r$  by comparing the extinction time of the first gene by running a simulation with a large threshold  $T = 250000$ . We would like to note that for the ideal mean-field case, the extinct gene can always come back in the future, so the scaling of  $r_c^g$  appearing in Fig. S6 works as an ideal case to compare with other cases and examine our theory.

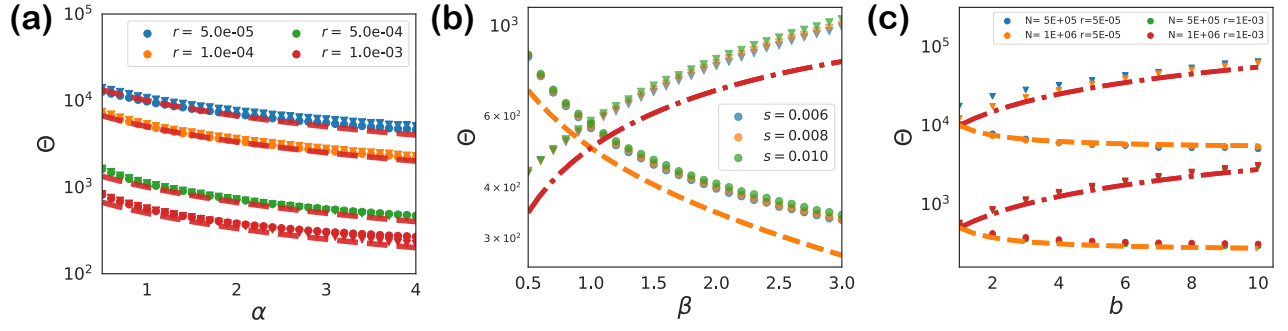


FIG. S7. Effective genotype temperature  $\Theta$  for hosts and phages with (a) different HGT rates, (b) interaction strength and (c) population size. The dashed lines and dash-dotted lines are predictions from the theory for hosts and phages respectively. The scatter points are simulation data with  $L = 40$ ,  $r = 10^{-3}$ ,  $s = 5 \times 10^{-3}$ , and  $N = 10^6$  unless specified. Circular and triangular markers represent hosts and phages, respectively.

HGT	Boom-bust cycles		Stochastic oscillator	
	$\Theta$	$\theta$	$\Theta$	$\theta$
mean-field	$1/2r$	$1/2r$	$1/2r$	$1/2r$
host-host/ phage-host	$1/2r$	$1/2r$	$1/2r$	$2/r$
host-host/ phage-phage	$1/2r$	$1/2r$	$2/r$	$L/r$

TABLE I. Summary of effective temperature for different types of HGT.

### VIII: Distinct parameters for hosts and phages

In the main text, we set the ratios:  $\alpha = r_V/r_B$ ,  $\beta = s_V/s_B$ , and  $b = n_V^*/n_B^*$  all equal to 1 to reduce the parameter space. In nature we often anticipate the phage to have a larger clone size  $b > 1$ , a higher HGT rate  $\alpha > 1$ , and for the burst size, proportional to  $\beta$ , to be also larger than 1. Let's investigate how they affect the effective temperature in Regime III first.

#### 1. Regime III

In this regime, the dynamics become

$$\begin{aligned} \frac{dB}{dt} &= sB \left( 1 - \frac{V}{bn_G^*} \right) + rn_G^* + \sqrt{B}\eta_B, \\ \frac{dV}{dt} &= \beta sV(B/n_G^* - 1) + \alpha rbn_G^* + \sqrt{V}\eta_V, \end{aligned} \quad (\text{VIII1})$$

where  $s = s_B$ ,  $r = r_B$ , and  $N = N_B$ .

The Lyapunov function becomes

$$E = b(B - n_G^* \log \frac{B}{n_G^*}) + \frac{1}{\beta}(V - bn_G^* \log \frac{V}{bn_G^*}). \quad (\text{VIII2})$$

We define the effective temperature  $T$ , and the host, phage abundances follow

$$B \sim \text{Gamma}(n_G^*, \Theta_B = T/b), \quad V \sim \text{Gamma}(bn_G^*, \Theta_V = \beta T). \quad (\text{VIII3})$$

Repeating the above steps, the self-consistency equation is

$$\left\langle \frac{bn_G^*}{2B} + \frac{bn_G^*}{2\beta V} + br \frac{n_G^*(B - n_G^*)}{B} + \alpha r \frac{bn_G^*(V - bn_G^*)}{\beta V} \right\rangle_{\rho(B), \rho(V)} = 0. \quad (\text{VIII4})$$

After taking the average, it becomes

$$\frac{\beta(b - 2rT)}{bn_G^* - T} + \frac{(1 - 2\alpha\beta rT)}{bn_G^* - \beta T} = 0. \quad (\text{VIII5})$$

We drop the nonphysical solution and the other solution of  $T$  is a complicated expression:

$$T = \frac{b(\beta^2 + 2(1 + \alpha)\beta n_G^* r + 1) - \sqrt{b^2(\beta^2 + 2(\alpha + 1)\beta n_G^* r + 1)^2 - 8b\beta(\beta b + 1)n_G^* r(\alpha + \beta)}}{4\beta r(\alpha + \beta)}. \quad (\text{VIII6})$$

If we only change one pair of parameters and keep the other two identical, we find simpler expressions:

- Different gene exchange rate  $r$ :

$$\Theta_B = \Theta_V = \frac{1}{(1 + \alpha)r}. \quad (\text{VIII7})$$

- Different  $N$ :

$$\Theta_B = \frac{T}{b} = \frac{1 + b}{4br}, \quad \Theta_V = T = \frac{1 + b}{4r}. \quad (\text{VIII8})$$

- Different  $s$ :

$$\begin{aligned} \Theta_B &= \frac{1 + 4\beta n_G^* r + \beta^2 - \sqrt{1 + 2\beta^2 + 16\beta^2 n_G^* r(n_G^* r - 1) + \beta^4}}{4\beta(\beta + 1)r}, \\ \Theta_V &= \frac{1 + 4\beta n_G^* r + \beta^2 - \sqrt{1 + 2\beta^2 + 16\beta^2 n_G^* r(n_G^* r - 1) + \beta^4}}{4(\beta + 1)r}. \end{aligned} \quad (\text{VIII9})$$

We examine the above results with simulation in Fig. S7.

## 2. Summary

From the above calculations, we can see that these ratios cannot be simply canceled out through parameter rescaling because they may affect demographic noises and HGT processes non-trivially. This also brings some difficulties in evaluating the temperature in Regime II for a similar reason. However, qualitatively, when  $\alpha$ ,  $\beta$ , and  $b$  are greater than 1, it implies the phage tends to kill the booming host earlier, thereby reducing fluctuations in host abundances and lowering the temperature. For instance, an increase in the phage's HGT rate or population size can enhance its establishment probability due to the larger rebirth rate. As a consequence, we can expect the setting of  $\alpha, \beta, b > 1$  to shift the transition to a lower value of the bacterial HGT rate  $r$ , compared to the baseline case where  $\alpha$ ,  $\beta$ , and  $b$  are set to 1, as shown in Fig. S8. In essence, the natural settings ( $\alpha, \beta, b > 1$ ) promote the gene and genotype diversity, compared to our simplified settings ( $\alpha = \beta = b = 1$ ).

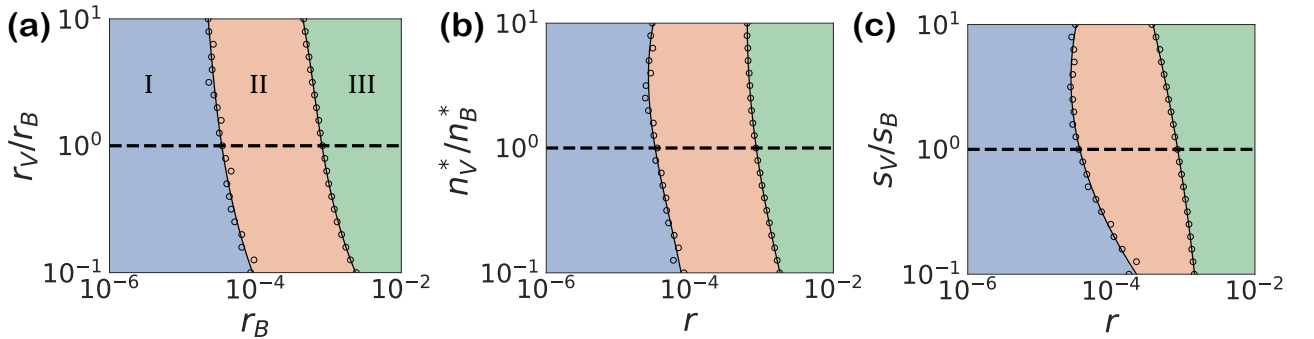


FIG. S8. Phase diagrams for phages and hosts with different ratios of HGT rates, fixed points, and phage death rate/host birth rate. The scatter points are the minimal HGT rates to keep gene and genotype diversity invariant over a simulation period  $T = 250000$ . The black solid lines are spline interpolation through the scatter points. The horizontal dashed line corresponds to the simplified case shown in Fig. 2 in the main text.

### IX: Transformation between the time and population distributions

In the host rising process, the host abundance grows exponentially with time:

$$n(t) = n_0 e^{st}, \quad dn = s n dt, \quad (\text{IX1})$$

where  $s$  is its fitness, and  $n_0$  is the initial population size at  $t = 0$ .

We would like to estimate the population distribution from the time distribution,

$$Q(n) = \int P(n|t)P(t)dt = \int \delta(n_0 e^{st} - n)P(t)dt = \int \delta(t - \frac{1}{s} \log \frac{n}{n_0})P(t) \frac{dt}{sn} = \frac{1}{sn} P(\frac{1}{s} \log \frac{n}{n_0}). \quad (\text{IX2})$$

Reverse this process, and recall the normalization:  $\int P(t|n)dt = 1$ ,

$$P(t) = \int P(t|n)Q(n)dn = \int s n_0 e^{st} \delta(n_0 e^{st} - n)Q(n)dn = s n_0 e^{st} Q(n_0 e^{st}). \quad (\text{IX3})$$

### X: Establishment probability with a constant fitness for two different processes

#### 1. Birth-death process

When the phage population is small, its targeted host's fitness is  $s$ . In a unit of time  $\Delta t$ , the host's birth probability is  $(1 + s)\Delta t$ , its death probability  $\Delta t$ , and the probability that neither happens is  $1 - (s + 2)\Delta t$ . With the basic extinction theory of branching processes, its extinction probability after  $t$  generations,  $w(t)$ , follows

$$w(t) = (1 - (s + 2)\Delta t)w(t - 1) + \Delta t + (1 + s)\Delta t w(t - 1)^2, \quad (\text{X1})$$

where we assume each birth event happens with two offspring. In the continuum limit,

$$\frac{dw}{dt} = 1 - (s + 2)w + (1 + s)w^2. \quad (\text{X2})$$

It is useful to rewrite in terms of the survival probability  $\phi(t) = 1 - w(t)$ :

$$\frac{d\phi}{dt} = s\phi - (1 + s)\phi^2. \quad (\text{X3})$$

In the long-time limit, it gives the establishment probability

$$\phi(\infty) = \frac{s}{1 + s} \approx s. \quad (\text{X4})$$

#### 2. Poisson process

In our simulation, we use the Poisson process instead of the birth-death process with two offspring. Instead of eq. (X1), the extinction probability after time  $t$  follows

$$w(t) = e^{-(s+1)\Delta t} \sum_{k=0}^{\infty} \frac{((s+1)\Delta t)^k}{k!} w(t - \Delta t)^k = e^{(s+1)\Delta t[w(t-\Delta t)-1]}, \quad (\text{X5})$$

where  $e^{-(s+1)\Delta t} \frac{(s\Delta t)^k}{k!}$  is the probability of having  $k$  offspring during a unit of time  $\Delta t$ , and  $w(t - \Delta t)^k$  is the probability that all  $k$  offspring go extinct after  $t - \Delta t$ .

The expression in terms of the survival probability is

$$1 - \phi(t) = e^{-(1+s)\Delta t \phi(t-\Delta t)}. \quad (\text{X6})$$

Assuming  $\phi(\infty)$  is small, and choosing  $\Delta t = 1$  in the simulation, the establishment probability is

$$\phi(\infty) = \frac{2s}{1 + 2s} \approx 2s. \quad (\text{X7})$$

Comparing with eq. (X4), our simulation set-up brings a factor of 2. We use the birth-death process in the weak HGT regime because it is easy to construct the partial differential equation (PDE) in the continuum limit. When comparing with the simulation, we will correct our theoretical results about the establishment probability by a factor of 2.



## XI: Supplementary figures

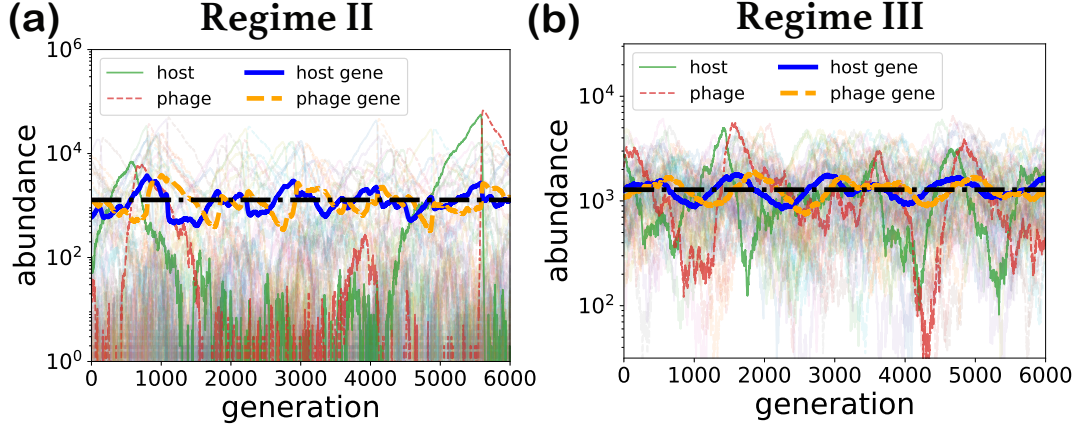


FIG. S9. Comparison between gene and genotype dynamics in Regime II (a) and Regime III (b). We show the population dynamics of one specific gene and multiple genotypes containing that gene. In order to compare gene and genotype abundance at the same scale, the gene abundance is divided by  $L - 1$ . The black dash-dotted line is the average of genotype abundances.

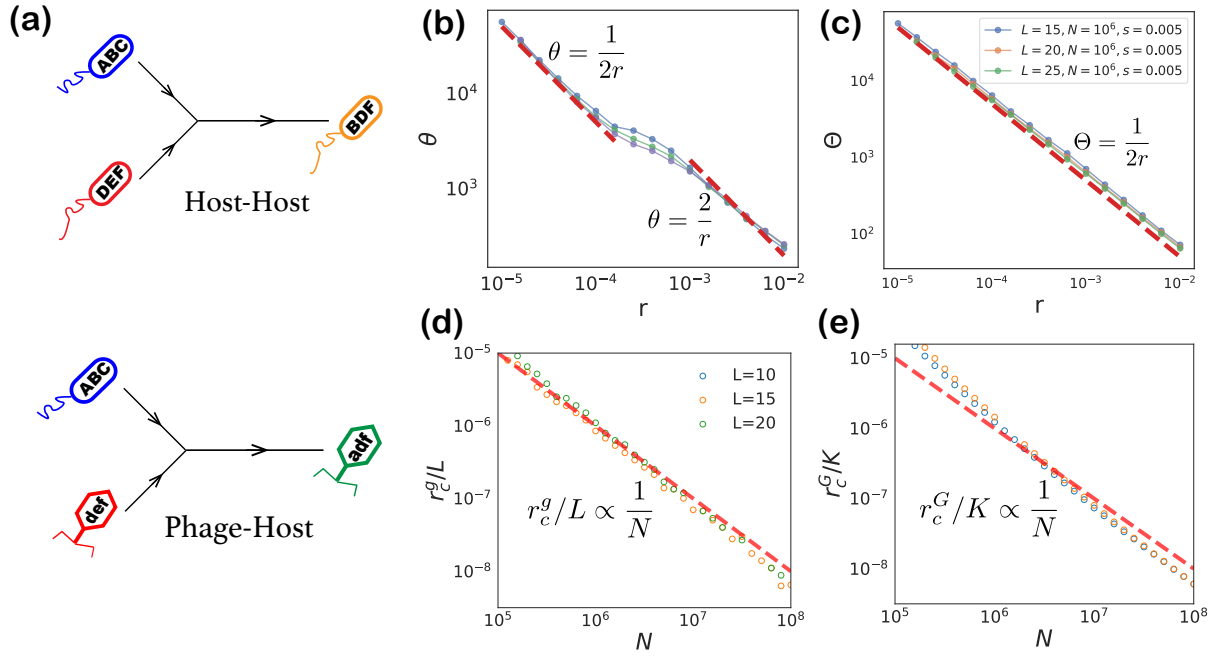


FIG. S10. (a) Scheme of host-host and phage-host HGT for "triplet". The phage and host can carry three different genes. There is one gene transferred in each HGT event. (b) Effective genotype temperature  $\Theta$  and (c) gene temperature  $\theta$  for "triplet". Critical HGT rates for (d) gene coexistence and (e) genotype coexistence for the "triplet" case. The red dashed lines are our theoretical predictions (the same as "doubleton" case).

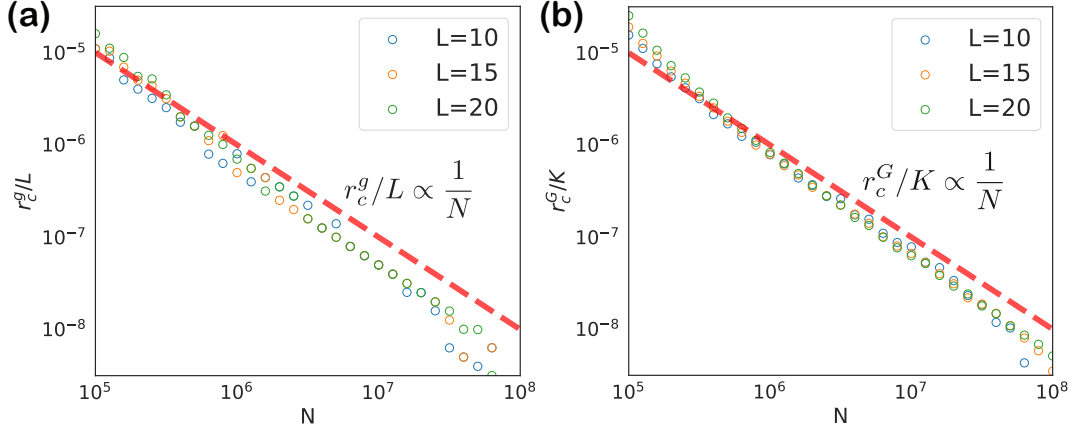


FIG. S11. Minimal HGT rates for gene coexistence (a) and genotype coexistence (b) for host-host and phage-host HGT without fixing the total population size. The red dashed line is our theoretical prediction, which shows the constraint of fixing the total population size does not affect our results in the main text.

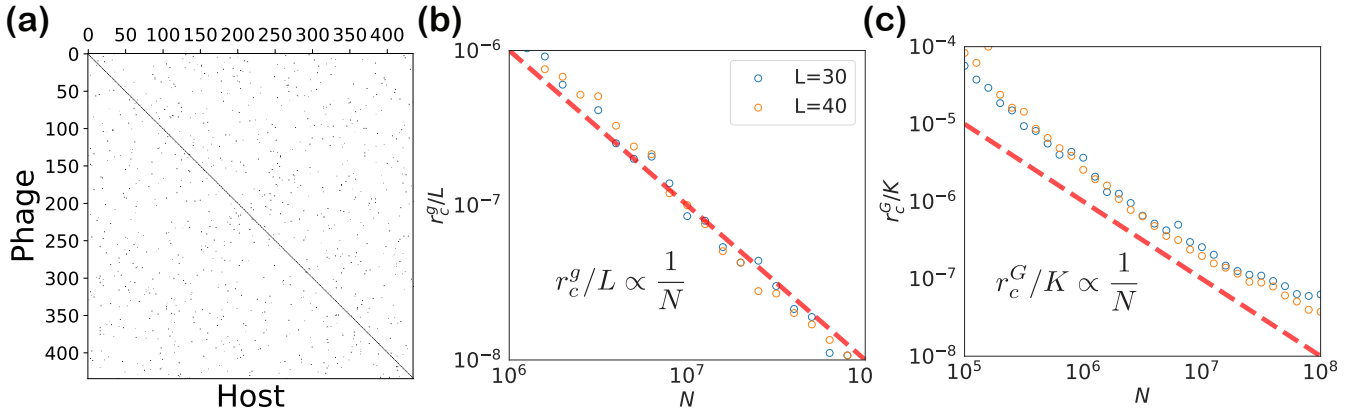


FIG. S12. (a) The heatmap for the binary sparse interaction matrix with  $L = 30$ . Each phage strain has the ability to infect another two random host strains beside the exact matching one. The  $y/x$ -axis are the labels of phages/hosts. The black points are the non-zero entries, indicating the phage can infect that host. (b, c) Minimal HGT rates for gene and genotype coexistence for host-host and phage-host HGT. The red dashed line is our theoretical prediction, which shows our theory can also be generalized to the sparse interaction structure.